Available online at www.sciencedirect.com
ScienceDirect
Geomorphology 100 (2008) 506–526
GEOMORPHOLOGY
www.elsevier.com/locate/geomorph

Decoding temporal and spatial patterns of fault uplift using transient river long profiles

Alexander C. Whittaker [a,*], Mikaël Attal [a], Patience A. Cowie [a], Gregory E. Tucker [b], Gerald Roberts [c]

[a] Grant Institute of Earth Science, School of GeoSciences, University of Edinburgh, West Mains Road, Edinburgh, EH9 3JW, Scotland, UK
[b] Department of Geological Sciences, University Of Colorado, Boulder, Co 80309-0399, USA
[c] Joint Research School of Earth Sciences, UCL-Birkbeck College, Gower Street, London, WC1E 6BT, UK

Received 5 July 2007; received in revised form 28 January 2008; accepted 29 January 2008
Available online 15 February 2008

Abstract

We present detailed observations of rivers crossing active normal faults in the Central Apennines, Italy, where excellent constraints exist on the temporal and spatial history of fault movement. We demonstrate that rivers with drainage areas >10 km^2 and crossing faults that have undergone an increase in throw rate within the last 1 My, have significant long-profile convexities. In contrast, channels that cross faults that have had a constant-slip rate for 3 My have concave-up profiles and have similar concavities and steepness indices to rivers that do not cross any active fault structures. This trend is consistent across the Central Apennines and cannot be explained by appeal to lithology or regional base level change. The data challenge the belief that active faulting must always be reflected in river profiles; instead, the long-profile convexities are best explained as a transient response of the river system to a *change* in tectonic uplift rate. Moreover, for these rivers we demonstrate that the height of the profile convexity, as measured from the fault, scales with the magnitude of the uplift rate increase on the fault; and we establish that this relationship holds for throw rate variation along strike for the same fault segment, as well as between faults. These findings are shown to be consistent with predictions of channel response to changing uplift rate rates using a detachment-limited fluvial erosion model, and they illustrate that analysis of the magnitude of profile convexities has considerable predictive potential for extracting tectonic information. We also demonstrate that the migration rate of the profile convexities varies from 1.5–10 mm/y, and is a function of the slip rate increase as well as the drainage area. This is consistent with $n>1$ for the slope exponent in a classical detachment-limited stream-power erosion law, but could potentially be explained by incorporating an erosion threshold or an explicit role for sediment in enhancing erosion rates. Finally, we show that for rivers in extensional settings, where the response times to tectonic perturbation are long (in this case >1 My), attempts to extract tectonic uplift rates from normalised steepness indices are likely to be flawed because topographic steady state has not yet been achieved.

Keywords: Rivers; Long profile; Tectonics; Faults

1. Introduction

The earth's landscape represents the time-integrated product of the interaction between tectonics and climate (Whipple and Tucker, 1999; Whipple, 2004). In principle, therefore, a temporal record of these competing signals will be recorded in landscape through the production or modification of a range of geomorphic features (Willett and Brandon, 2002; Anders et al., 2006; Wobus et al., 2006). This raises the prospect that by developing tools to decode this landscape record, we may gain access to a new archive of past tectonic and climatic signals, resolvable over the response timescale of the geomorphological feature studied and over a range of spatial scales. Amongst other things, this would allow us to improve our predictions of tectonic setting where direct structural or geodetic data are unavailable (Burbank and Anderson, 2001) and could be invaluable for refining hazard prediction (c.f., Roberts et al., 2004) and determining landscape sensitivity to future climate

* Corresponding author. Department of Earth Science and Engineering, Imperial College, London, SW7 2AZ, UK. Tel.: +44 79309 57816.
E-mail address: a.whittaker@imperial.ac.uk (A.C. Whittaker).

0169-555X/$ - see front matter © 2008 Elsevier B.V. All rights reserved.
doi:10.1016/j.geomorph.2008.01.018

change (e.g., Molnar, 2001; Roe et al., 2002). Moreover, the growing availability of high-resolution digital elevation models (DEMs) in combination with sophisticated GIS software has revolutionised our ability to probe and quantify present-day topography, and seemingly provides the detailed data sets required to bring this goal within reach (Tarboton et al., 1991; Wobus et al., 2006).

Despite these technical advances, we remain a considerable distance away from achieving these aims. Firstly, the interaction between climate, tectonics, and landscape is complex and non-linear over a range of time periods, making the isolation of any one of these signals difficult (Molnar and England, 1990; Finlayson et al., 2002; Dadson et al., 2003; Montgomery and Stolar, 2006). Secondly, to extract information on tectonics or climate from discrete geomorphological features requires us to have detailed knowledge of how the long-term physical behaviour of landscape systems is expressed in the time-integrated morphologies they produce (Whipple and Tucker, 1999). For example, we already know that some key surface systems, such as hillslopes, rapidly reach threshold gradients in areas of high uplift rate (Tucker and Bras, 1998; Montgomery, 2001) or where the rate of soil production is rapid (Roering et al., 1999), limiting their sensitivity to changes in boundary conditions, and hence restricting their use to specific climate or tectonic environments. In contrast, the upland river system has become the major focus for study in this area (e.g., Lavé and Avouac, 2001; Snyder et al., 2000, amongst many others) because over length scales >1 km, the earth's surface is channelised and consequently the fluvial network acts as the primary agent by which tectono-climatic signals are transmitted to landscape as a whole (Merrits and Vincent, 1989; Whipple and Tucker, 1999; Whipple, 2004). Moreover, because aspects of channel form (such as streamwise gradients, channel geometry, etc.) remain sensitive, at least to tectonics, over timescales >1 My (Whittaker et al., 2007a,b) and key attributes (such as channel lengths, slopes and drainage areas) are easily extractable from DEM data, the fluvial system is widely accepted to be the most fruitful area for landscape analysis (c.f. Wobus et al., 2006).

In this paper, we focus on the study of upland rivers to deduce tectonic signals over time periods $>10^5$ years. In particular, we examine how river long profiles and drainage networks reflect relative rates of rock uplift by documenting fluvial response to active faulting in the Central Apennines of Italy, where excellent constraints exist on the long-term displacement rates of the active normal faults that dominate the topography of the area (Roberts and Michetti, 2004). By comparing rivers crossing faults with different slip rates, and also differing temporal histories of slip, we quantify, for this system, the conditions under which river long profiles can be used to extract tectonic signals from landscape; and we compare our results to predictions of river response to differential uplift using the CHILD landscape evolution model (Tucker et al., 2001). We establish that transient landscapes (i.e., *not* in topographic steady state) can act as a tectonic archive over time periods >1 My, but our results show that caution is required when using normalised steepness indices (c.f. Wobus et al., 2006) as a proxy for rock uplift rate in areas of active tectonics.

2. Previous work

To extract tectonic signals from any fluvially mediated landscape, we need to understand the long-term erosional dynamics of the upland rivers (Whipple, 2004). Work toward this goal has largely focused on formulating erosion "laws" for catchments in areas assumed to be in "equilibrium" or topographic steady state (here used to mean that the rate of tectonically controlled uplift equals the rate of erosional downwearing) (Howard and Kerby, 1983; Howard et al., 1994; Seidl et al. 1994). The stream-power erosion model is the most durable result of these enquiries, casting the incision rate, E, of a channel into bedrock as a function of just two main variables, the river slope, S, and discharge, Q (or more commonly, the upstream drainage area, A, as a proxy):

$$E = KA^m S^n \tag{1}$$

K is a parameter that subsumes other relevant factors, such as substrate erodibility, and the exponents m, n are determined by the precise erosion law chosen e.g., for erosion rate proportional to basal shear stress, $m=1/3$, $n=2/3$ (Howard and Kerby, 1983), while for potential energy expenditure per unit channel area, $m=0.5$, $n=1$ (Tucker and Whipple, 2002). A and S are readily extractable from DEMs, and by assuming that the rate of uplift in an area is balanced by the rate of stream-power driven incision Eq. (1), we obtain

$$S = k_s A^{-\left(\frac{m}{n}\right)} \tag{2}$$

where the pre-factor, k_s (the steepness index), of the channel now subsumes information about uplift as well as the parameter K from Eq. (1) (Snyder et al., 2000), and the ratio m/n is called the *concavity* (usually given the symbol θ). The power-law dependence of river slope and drainage area is well-established for $A>1$ km^2 (Montgomery, 2001), and both k_s and θ can be readily estimated from log–log plots of slope and drainage area, which have gained widespread use in the geomorphic literature. Concavities depend on the long-term erosional dynamics of the channel, and documented values are generally $0.2<\theta<1$, with 0.5 considered typical (Hack, 1957; Sklar and Dietrich, 1998; Stock and Montgomery, 1999). They exert a fundamental control on river long profiles (i.e., channel elevation against distance downstream, L), because L itself is a power-law function of drainage area (e.g., $L \approx kA^{0.5}$, Hack, 1957). By substituting this relationship into Eq. (2) and integrating with respect to L, one can easily demonstrate that most channels should exhibit a concave-up longitudinal profile if they are in topographic steady state and K does not vary across the catchment.

Consequently, most researchers trying to extract tectonic signals from landscape have focused on documenting deviations from "ideal" concavities or trends in the steepness index, k_s between or along rivers, which are not easily explained by appeal to differing lithology. For example, Kirby and Whipple (2001) analysed channel response to spatial gradients in uplift rate, and predicted from theoretical considerations that channels flowing towards a zone of increasing uplift should have reduced

concavities, whereas if uplift rates decrease downstream, channel concavities should be significantly elevated. They tested this idea using data from the Siwaliks Hills, Central Nepal, in order to quantify differential uplift rates, but concluded that the analysis was hampered by confounding factors such as lithology, glaciation, and differing sediment flux. Moreover, their analysis only permits variations in slope to drive incision rates, whilst similar data to the east in Tibet, which accommodates convergence of 2–3 mm/y suggest that channel concavities in this area are not demonstrably different from regions that have uniform uplift rates (Kirby et al., 2003). However, these Tibetan rivers do apparently show significant variations in steepness index towards the plateau margin that they interpreted as an area of active rock uplift, although they do not have the data to demonstrate this unequivocally. A number of authors (e.g., Duvall et al., 2004, Wobus et al., 2006) strongly advocate the use of "normalised" steepness indices, k_{sn}, based on the premise that reference concavities can be used to define standard steepness values that characterise a region. They have shown that data from the King Range, San Gabriel and Santa Ynez mountains, California, are all consistent with channel steepness set by uplift rate, and Wobus et al. (2006) was able to identify a linear relationship between k_{sn} and predicted rock uplift rates in Central Nepal, based on a data set of seven channels, and a fault-bend-fold kinematic model of uplift.

Although this approach has proven to be a useful tool in the above settings, the link between steepness indices and tectonic uplift rates appears to be considerably more equivocal in other areas (Hurtrez et al., 1999; Snyder et al., 2000). Firstly, this type of analysis is very sensitive to the reference concavity chosen, and depends on the somewhat arbitrary selection of "undisturbed" channel segments (i.e., those that do not display oversteepened or convex reaches, or cross documented gradients in uplift rate) where slope changes are dispersed over more than one order of magnitude in drainage area. Moreover, the idea that steepness index will reflect the rate of uplift implicitly assumes that the landscape is in topographic steady state. However, given that we are considering landscapes *responding* to tectonic forcing, there is no guarantee that such an equilibrium has been achieved (c.f. Gasparini et al., 2006; Whittaker et al., 2007a). Indeed, a key result from landscape modelling to date is that rivers near to the detachment-limited end member can be expected to show deviations from "equilibrium" concave-up profiles when perturbed by tectonics (Tucker and Whipple, 2002; Whipple and Tucker, 2002). In response to a relative increase in uplift rate, a knickzone, or convex reach in the profile develops that separates the lower-part of the catchment (which is adjusting to the new uplift signal) from the upper part (which is yet to feel the effects of the relative uplift rate change) and so is not in topographic steady state. Over time, the knickzone migrates up the river channel and hence establishes a new 'equilibrium' configuration. In contrast, transport-limited systems can be expected to display a diffusive style of behaviour (Tucker and Whipple, 2002; Whipple and Tucker 2002) and are not expected to develop significant long-profile convexities.

One implication of the above is that it is difficult using conventional slope-area analysis to distinguish between detachment-limited rivers with long-profile convexities produced by (i) transient response to base level fall or change in fault slip rate, from (ii) channels crossing from one uplift zone to another, but having achieved topographic steady state (Kirby et al., 2003; Wobus et al., 2006). Consequently, if we are to succeed in using fluvially shaped landscapes to deduce information about tectonics, we need first to characterise channel response to tectonic forcing where we do not *assume* topographic steady state, and where the boundary conditions are well-constrained independently. We tackle this issue using a data set from Italy where the tectonic framework is uniquely well constrained (Section 3) and where previous work has characterised at least one catchment undergoing a transient response to tectonics (Whittaker et al., 2007a).

3. Tectonic setting

The Central Apennines of Italy is a region of extending continental crust positioned within the zone of convergence between the Eurasian and African Plates (D'Agostino and Jackson, 1999; Roberts and Michetti, 2004). The Apennines represent a north-east verging imbricate fold and thrust belt that formed as a result of this convergence, and thrusting continues to the present day on the Adriatic side of the mountain chain. However, in Central Italy, thrusting ceased by the lower Pliocene (Patacca et al., 1990; Pizzi, 2003; Centamore and Nisio, 2003) and since this time (ca. ~3 Ma), a zone of extension has formed behind the compressional front, (Fig. 1A) arguably driven by roll-back of the Calabrian subduction zone (Lavecchia et al., 1994, D'Agostino et al., 2001). This has produced a network of high angle normal faults (Fig. 1B), over 150 km in length, which accommodates stretching of ~6 mm/y across Central Italy (Hunstad et al., 2003; Roberts and Michetti, 2004). The normal faults uplift platform carbonates, largely of Mesozoic age, while the associated half-grabens are underlain by Miocene flysch bedrock (Accordi et al., 1986). These grabens are now filled by continental deposits (dated in places to >2.5 Ma) that are considered contemporaneous with the onset of extension (Fig. 1B) (Bosi and Messina, 1991; Cavinato, 1993; Cavinato and De Celles, 1999; Cavinato et al., 2002). Although there is ample sedimentological evidence that much of the Central Apennines lay at or near sea-level in the late Pliocene (Centamore and Nisio, 2003), the area is now uplifted on the back of a long-wavelength topographic bulge, thought to be supported dynamically by mantle convection (D'Agostino and Jackson, 1999). This has resulted in many basins having minimum elevations >500 m, with the highest peaks at altitudes >2000 m (Fig. 1C). As most of the NW striking range fronts are bounded by faults (Fig. 1B,C), the fault array has therefore played a controlling role in the development of both differential relief and drainage in the Central Apennines, (see D'Agostino et al., 2001). This makes the area an ideal laboratory to study the effect of tectonics on the fluvial network.

The Apennine fault array is also one of the best constrained in the world in terms of documented spatial variation in both displacement and slip rate along each of the fault strands. Total accumulated throw for each of the faults is readily estimated

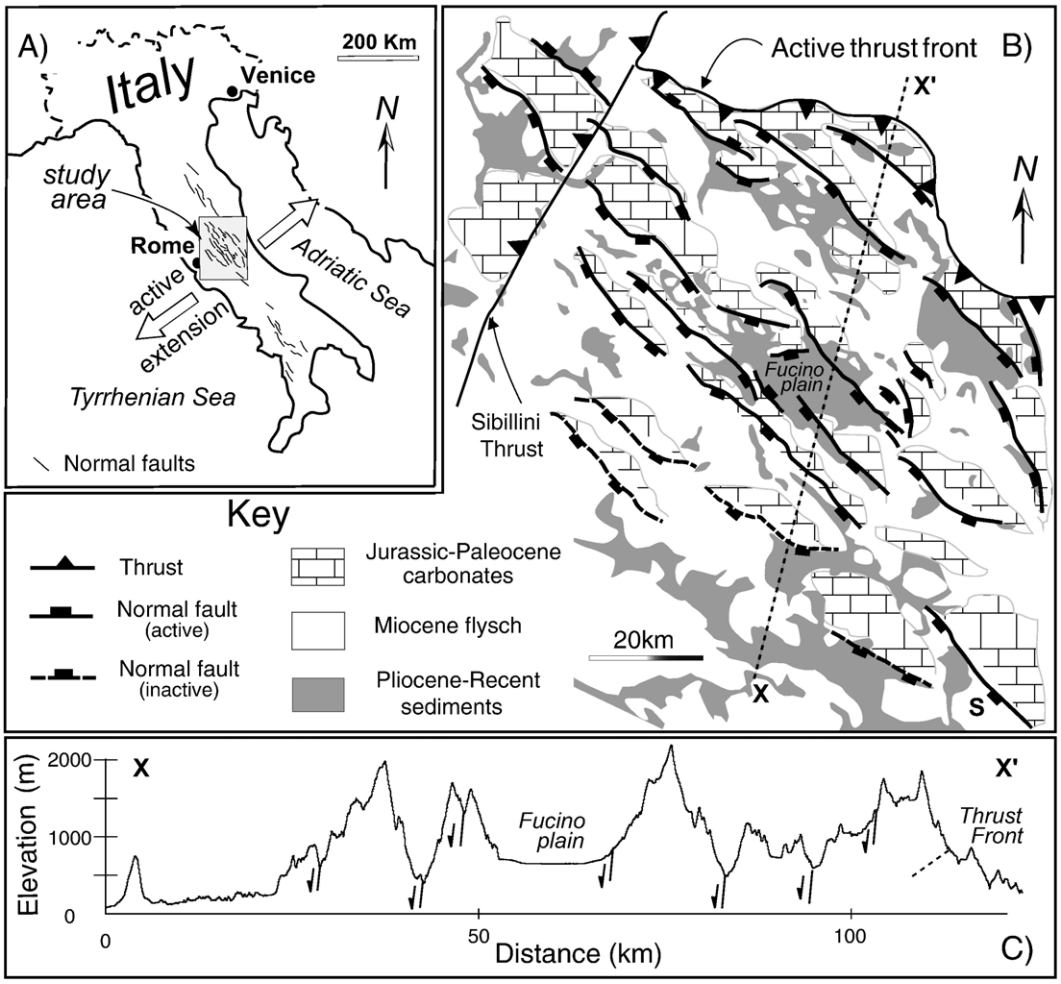

Fig. 1. (A) Inset map of Italy showing documented active normal faults. Grey box depicts study area shown in detail in B. (B) Geological and structural map of the Central Apennines, showing the location of thrusts and active normal faults, and their relation to lithology. (C) Topographic cross section (along line X–X'; B), demonstrating that the Apennine mountains form a long-wavelength topographic bulge, with minimum elevations >500 m for much of the area. Most of the range fronts are bounded by active normal faults.

from the offset of geological horizons (Roberts and Michetti, 2004), and current uplift rates have been estimated from (i) the size of fault scarps displacing late glacial hillslope surfaces (Giraudi and Frezzotti, 1997; Morewood and Roberts, 2002; Roberts and Michetti, 2004), (ii) trench sites across fault strands (e.g. Michetti et al., 1996; Pantosti et al., 1996), (iii) integrated seismic and borehole surveys (Cavinato et al., 2002) and (iv) surface exposure dating using cosmogenic nucleides (Palumbo et al., 2004). Fig. 2 demonstrates the quality of the tectonic data for this area. Fault throw and throw rates vary across the array, with the largest values (throw >2 km; rate ~2 mm/y) documented on faults in the centre of the array (zone B, Fig. 2). Slip rates <0.4 mm/y are documented for faults at the north and south edges of the array, and distally located faults on the far west of the Apennines show no Holocene displacement at all. Additionally, the data demonstrate that slip rates vary along strike on the same fault with maximum values at the strike centre and a mapped decline towards the fault tips (Morewood and Roberts, 2002; Roberts and Michetti, 2004).

There is also good evidence that the throw rate on some of the faults has varied through time: High slip rate faults near the centre of the array have comparatively low total displacements (typically 1.5–2.3 km, Figs. 2 and 3); therefore the assumption of constant-slip rate through time would require basin initiation ages younger than the age of known basin fill sediments (Cowie and Roberts, 2001). Consequently, throw rates on central fault segments must have increased (Roberts and Michetti, 2004) (Fig. 3A). In contrast, faults near the edge of the array have throw rates that are consistent with their total displacement, so have maintained approximately constant-slip rate through time. These observations are explained by elastic interaction between the growing faults, within a soft-linked fault array (Cowie and Roberts, 2001). This interpretation is directly supported from seismic data (see Cavinato et al., 2002) from the centrally-located Fucino basin. Our analysis of Cavinato et al.'s data (Fig. 3B) shows much thicker sediment sequences dipping toward the active fault from the mid-Pleistocene onward (sequence 4) than from late Pliocene–Early Pleistocene times (sequence 3). In this locality, which is south of the peak in maximum displacement on the fault, (Fig. 2), the current slip rate (measured from trench sites) is up to 1.5 mm/y and a 0.5 Ma tephra layer documented in the basin (Cavinato et al., 2002)

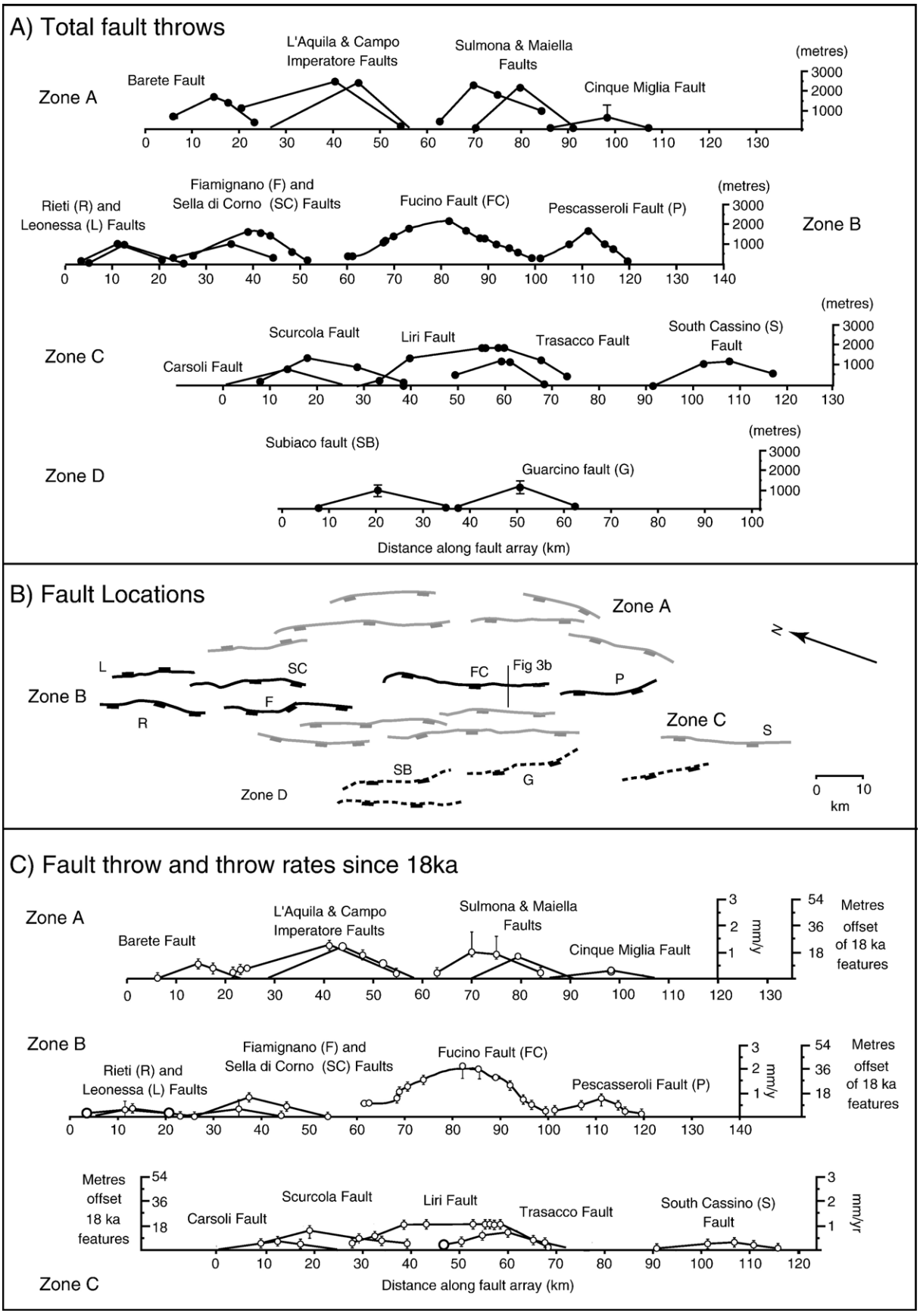
A) Total fault throws
Zone A
Barete Fault
L'Aquila & Campo Imperatore Faults
Sulmona & Maiella Faults
Cinque Miglia Fault
(metres)
3000
2000
1000
0 10 20 30 40 50 60 70 80 90 100 110 120 130
Zone B
Rieti (R) and Leonessa (L) Faults
Fiamignano (F) and Sella di Corno (SC) Faults
Fucino Fault (FC)
Pescasseroli Fault (P)
(metres)
3000
2000
1000
0 10 20 30 40 50 60 70 80 90 100 110 120 130 140
Zone C
Carsoli Fault
Scurcola Fault
Liri Fault
Trasacco Fault
South Cassino (S) Fault
(metres)
3000
2000
1000
0 10 20 30 40 50 60 70 80 90 100 110 120 130
Zone D
Subiaco fault (SB)
Guarcino fault (G)
(metres)
3000
2000
1000
0 10 20 30 40 50 60 70 80 90 100
Distance along fault array (km)
B) Fault Locations
Zone A
N
L
SC
FC
Fig 3b
P
Zone B
F
R
Zone C
S
SB
G
Zone D
0 10
km
C) Fault throw and throw rates since 18ka
Zone A
Barete Fault
L'Aquila & Campo Imperatore Faults
Sulmona & Maiella Faults
Cinque Miglia Fault
3
2
1
mm/y
54
36
18
Metres offset of 18 ka features
0 10 20 30 40 50 60 70 80 90 100 110 120 130
Zone B
Rieti (R) and Leonessa (L) Faults
Fiamignano (F) and Sella di Corno (SC) Faults
Fucino Fault (FC)
Pescasseroli Fault (P)
3
2
1
mm/y
54
36
18
Metres offset of 18 ka features
0 10 20 30 40 50 60 70 80 90 100 110 120 130 140
Metres offset 18 ka features
54
36
18
Carsoli Fault
Scurcola Fault
Liri Fault
Trasacco Fault
South Cassino (S) Fault
3
2
1
mm/yr
0 10 20 30 40 50 60 70 80 90 100 110 120
Zone C
Distance along fault array (km)

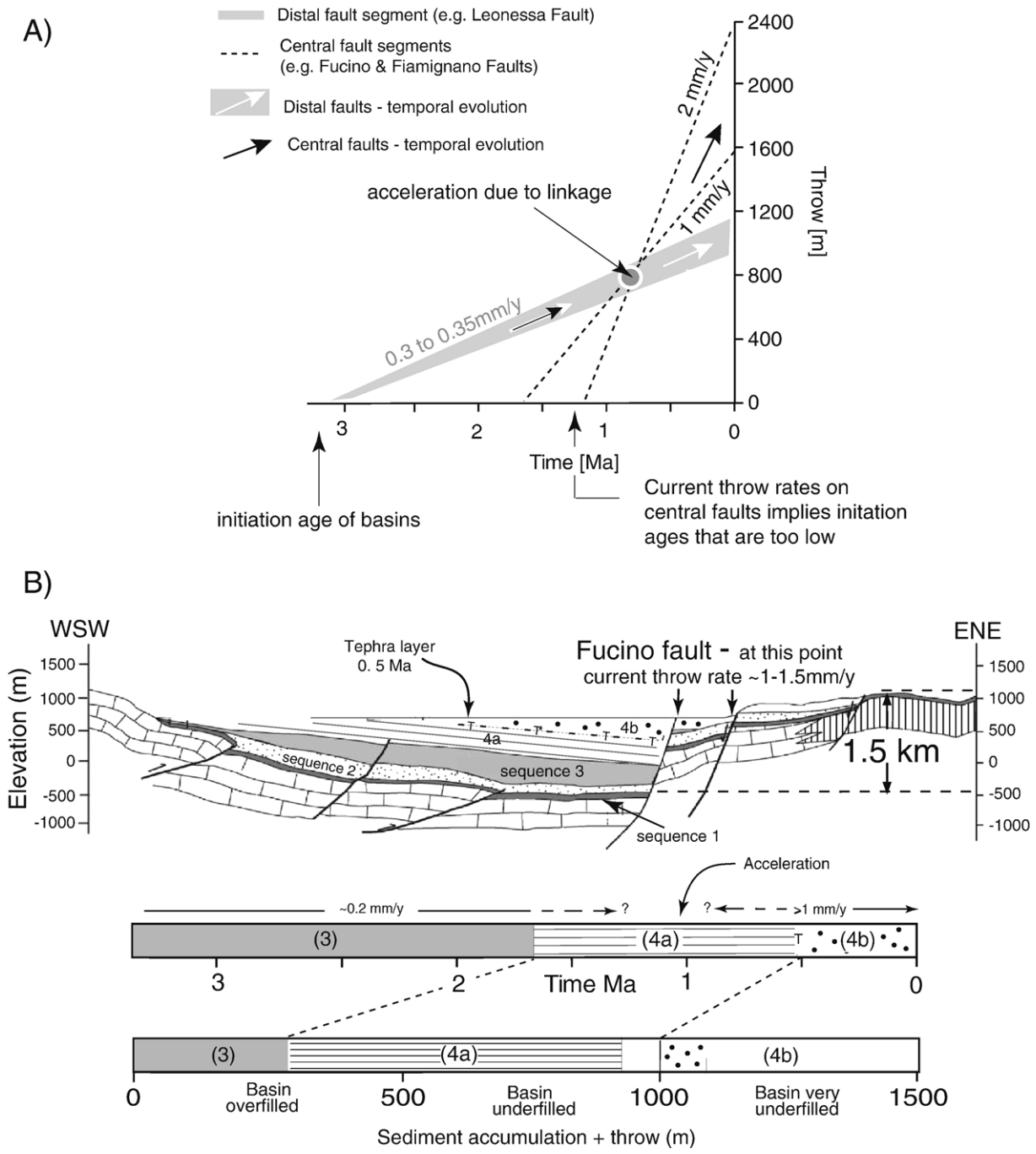

Fig. 3. (A) Accumulation of throw with time for central fault segments (e.g. Fucino (FC) and Fiamignano (F) faults) compared with distal segments (e.g. Leonessa fault, (L)). Centrally-located faults have current throw rates that imply fault initiation ages that are too young, implying slip rates are higher now than they were in the past. Distal faults have total throws consistent with a constant slip rate of 0.3 mm/yr for 3 My. (B) Reconstructed section across the internally drained Funcino plain (adapted from Cavinato et al., 2002) showing that sediments thicken into the Fucino fault. Bar charts show the three major syn-sedimentary sequences in terms of time and sediment thickness. Note that post-Early Pleistocene deposits (sequences 4a and 4b) are ~3× as thick as all the sediment accumulated during the Pliocene (sequence 3). White space shows unfilled accommodation space (basin was a lake until drained in 1874). The increase in accommodation generation occurred prior to 0.5 Ma, and likely after 1 Ma, consistent with the data in Fig. 3A, and modelling work (Cowie and Roberts, 2001).

Fig. 2. (A) Total fault throws (defined as *vertical* displacement on the fault) for active and inactive faults in the array, for four zones across the Apennines, shown in B. Data synthesised from Roberts and Michetti (2004), Papanikolaou et al. (2005), and geological maps of the area (Accordi et al. 1986). (B) Fault location map, showing zones used for throw and throw rate profiles in A and C, plotted at an identical horizontal length scale. Letters correspond to faults explicitly mentioned in Fig. 4 and in Sections 4–7 of the text. Note that spacing of the faults has been compressed by a factor of 1.5 in the direction NE-SW. (C) Present-day fault throw rates for zones A–C, primarily derived from Roberts and Michetti (2004), with additional measurements from Papanikolaou et al. (2005). The faults in zone D are presently inactive.

suggests a slip rate of at least 1 mm/y on average over this time. However, for the relatively thin sequence of Pliocene–Early Pleistocene sediments (seq. 3, Fig. 3B), accommodation generation could have been no more than 0.2 mm/y; and as well data documents coarse gravels and conglomerates, there is good evidence to suggest that the basin was filled at this time (Cavinato

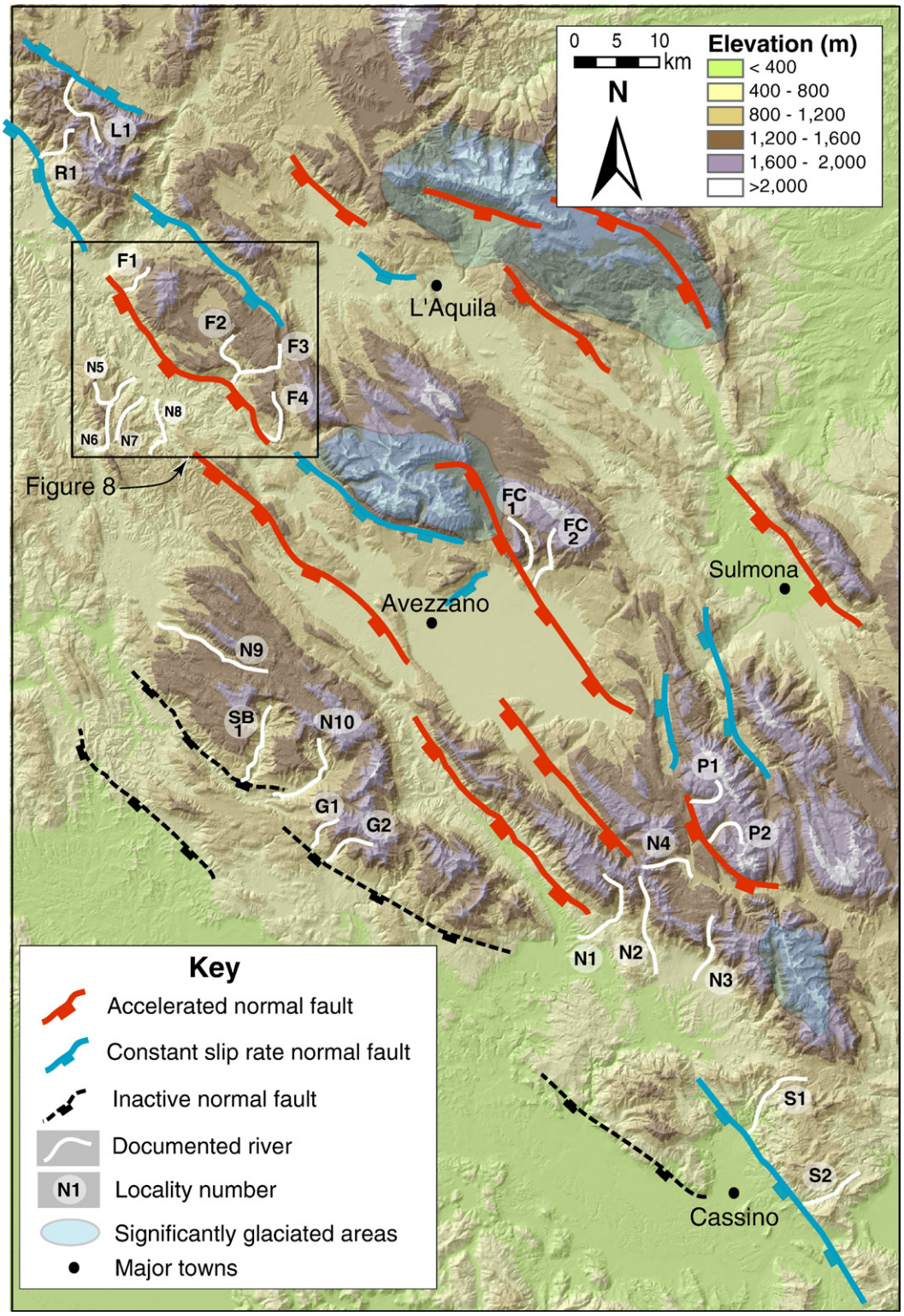

Fig. 4. DEM image, contoured for elevation, showing study localities of rivers >10 km^2 in drainage area across the Apennines. Dark blue depicts constant-slip rate faults; red — accelerated-rate faults; black — inactive faults. Light blue shading shows heavily glaciated areas excluded from analysis. L — Leonessa fault; R — Rieti fault; F — Fiamignano fault; FC — Fucino fault; P — Pescasseroli fault; S — South Cassino fault; G — Guarcino fault; SB — Subiaco fault. Box depicts detailed study area shown in Fig. 8.

et al., 2002). In contrast, sequence 4b is entirely dominated by lacustrine muds, so the basin by this time was significantly underfilled. An increase in throw rate must therefore have occurred during the deposition of sequence 4a; and we estimate on this basis the total fault throw is consistent with ~0.2 mm/y of slip until ~0.8 Ma, followed by ~1.1 mm/y since then. We also note that the increase in slip rate for central faults should result in the switching off of other fault segments, if the total rate of extension across the Apennines is to remain constant. This is what we observe in the west of the array, where there are a number of presently inactive faults, but with total throws of >700 m, which is consistent with a slip rate of ~0.3 mm/y for 2.25 My, followed by fault death once slip rate increase had ensued on centrally-located fault segments (zone D, Fig. 2). A synthesis of geological data and fault interaction theory (c.f., Cowie and Roberts, 2001) strongly suggests the acceleration in throw rate occurred at ~0.8 Ma (Roberts and Michetti, 2004).

4. Methodology

4.1. Approach

Using the wealth of detailed tectonic data outlined above, a 20 m resolution digital elevation model (DEM) of the Central Apennines, and field reconnaissance of key study sites, we are able to identify rivers that have been exposed to the following long-term tectonic settings:

(i) Channels crossing active faults, with a *constant-slip rate* since fault initiation at ~3 Ma.
(ii) Channels crossing active faults, with an *increase in slip rate* at ~0.8 Ma
(iii) Channels crossing faults with *no evidence of Holocene activity*, but which initiated at 3 Ma and were active during the Pleistocene.
(iv) Channels draining high topography that is not fault-bounded, but with identical lithology to the uplifted fault blocks.

We first utilize this data set to critically compare and contrast the long profiles and morphology of channels in the same field area that have experienced differing tectonic uplift fields through time (Section 5). Secondly, we then evaluate the extent to which our results (i) might be decoded to gain information about tectonic forcing from the landscape and (ii) are consistent with predictions of river response to changing uplift rates using the CHILD landscape model (Section 6).

4.2. Selection of study rivers

Because it is well known that the existence of a "river" on a DEM-derived stream network does not necessarily correlate with the existence on the ground of a real channel scoured by fluvial processes, we applied the following criteria in selecting catchments to study: Firstly, for footwall rivers crossing faults, we only selected channels with drainage areas ≥ 10 km^2 and downstream distances ≥ 5 km at the fault. Although this excludes a large number of small catchments draining the proximal footwall faces of the active faults in the area, channels in the Apennines smaller than this threshold display low concavities and steep long profiles (local slopes $\gg 5°$), morphologies which are typically associated with debris flow action rather than fluvial processes (Stock and Dietrich, 2003; Lague and Davy, 2003). Field inspection confirmed that these channels were indeed steep gulleys dominated by mass flows. Secondly, for the subset of channels that passed the above test, we used field observation to verify that they exhibited one or more of the following diagnostic features: running water or evidence of recent flow, fluvial abrasion marks, and evidence of active sediment transport. Lastly, we excluded channels that (i) had been heavily modified by damming/bank stabilisation work (ii) had been clearly dominated by glacial erosion, or (iii) where there was evidence of river capture (e.g., presence of wind-gaps linking a palaeo-channel to a neighbouring catchment).

Fig. 4 shows the localities of the 25 river channels throughout the Central Apennines selected for study using the criteria outlined. Eight of these (F1-4, FC1-2, P1-2) cross active normal faults (Fiamiginano, Fucino, and Pescasseroli, respectively; Fig. 3) which have undergone an increase in slip rate, four (L1, R1, S1-2) incise the footwalls of constant-slip rate faults (Leonessa, Rieti, and South Cassino), three (G1-2, SB1) cross presently inactive faults (Guarcino and Subiaco) and 10 cross high topography but no faults (N1-10). For each case, we extracted channel long profiles, and where appropriate also evaluated both the steepness index, k_s, and the normalised steepness index, k_{sn}, assuming a reference concavity of 0.5 Eq. (2). Additionally we documented lithology for each of these rivers, and in many cases augmented this with in situ measurements of rock mass strength following the Selby rock mass strength protocol (Selby, 1980). This approach synthesises field measurements of intact compressive rock strength using a Schmidt hammer with detailed assessments of joint orientation, size, spacing, and continuity. Additionally, it includes an evaluation of weathering degree. Resulting values lie on a scale from 0–100, with values <25 corresponding to soils. The approach is more robust than Schmidt hammer rebound measurements alone because rock resistance to erosion is significantly affected by the presence or absence of pervasive jointing (Whipple et al., 2000).

5. Results

5.1. Comparison between faults in the Apennines

Fig. 5A shows seven rivers with drainage areas between 18 and 65 km^2 crossing faults that have undergone an *increase* in uplift rate within the last million years. We note that, significantly, none of these channels display typical 'concave-up' long profiles. Instead, they all display prominent profile convexities that start above the fault. The effect is most noticeable for rivers crossing faults with the highest documented slip rates today (e.g. channels FC1 and FC2), and which therefore have undergone the largest slip rate increase (for the Fucino fault, >5× slip rate increase since 0.8 Ma (Fig. 3A,B)). This

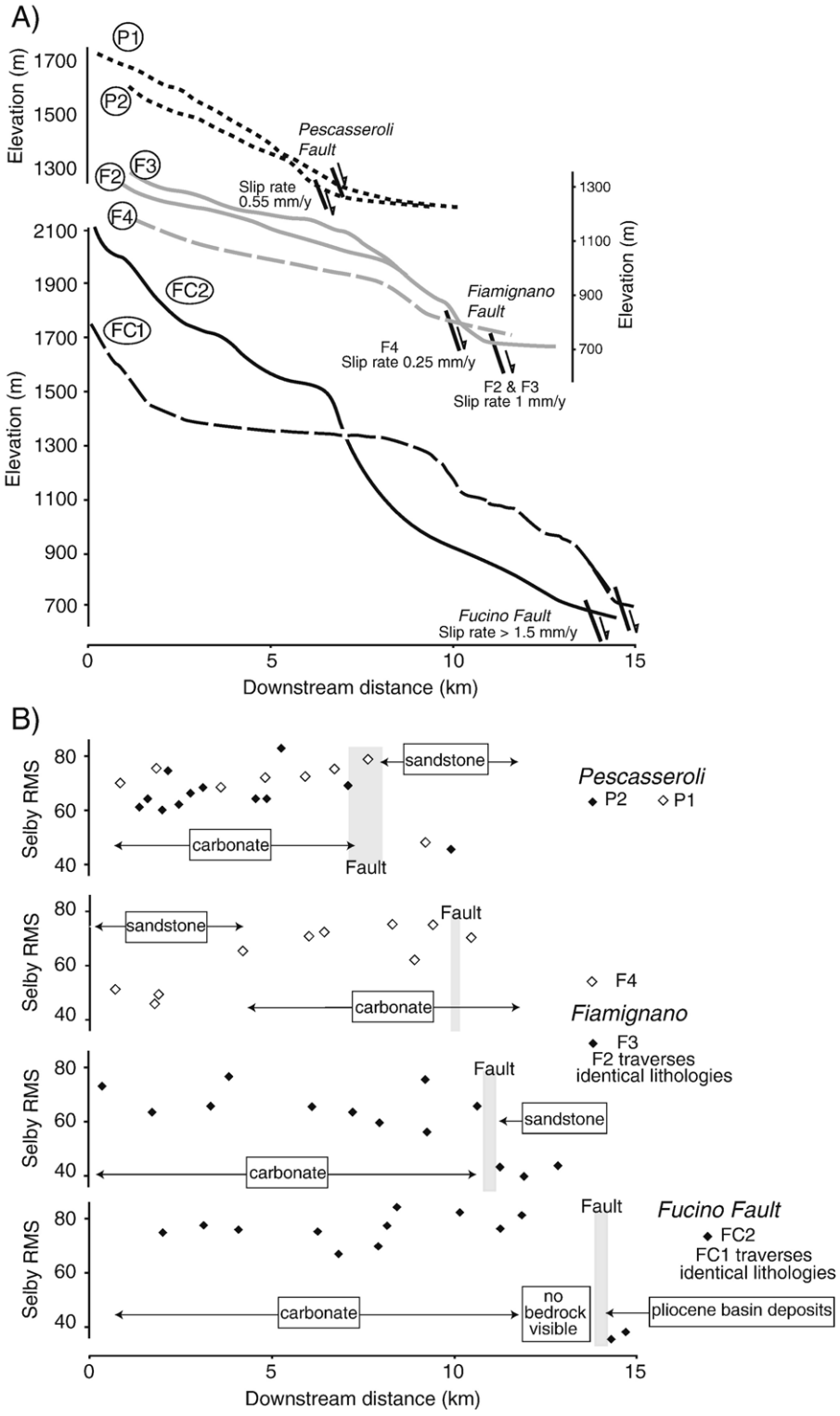

Fig. 5. (A) Examples of channel long profiles for rivers crossing faults that have undergone an acceleration in slip rate within the last 1 My. Locality numbers are shown geographically in Fig. 4. (B) Selby rock mass strength data (after Selby, 1980) against downstream distance for the catchments shown in Fig. 5A.

phenomenon appears to be systematic and cannot be explained by changing lithology or rock mass strength (RMS). In each case, the prominent break in slope in the channel long profile does not correlate with any change in Selby RMS or lithology (Fig. 5B). This is particularly true of channel F4, where the transition from sandstone to limestone in the upper part of the catchment does not coincide with any profile steepening, while the fault juxtaposes two limestones of identical rock strength. Nevertheless, the profile convexity starts immediately above the fault. These observations therefore rule out changing bedrock

resistance to erosion as an explanation for profile steepening (c.f. Stock and Montgomery, 1999; Whittaker et al., 2007a).

It is particularly instructive to compare these profiles with rivers of similar drainage area, incising similar lithologies but crossing constant-slip rate faults (Fig. 6). In this case, we note that these rivers do not display the significant convex reaches that characterise *all* the profiles in Fig. 5, despite crossing active faults with slip rates up to 0.4 mm/y. Instead, the profiles are concave-up, with $0.41<\theta<0.54$, similar to steady-state or equilibrium channels (Snyder et al., 2000; Whipple and Tucker, 2002). Additionally, we note there is no statistical difference in the concavity of these profiles compared to those crossing inactive faults (also shown on the same figure). Although there are considerable variations in steepness index, k_s, for these rivers, this is largely a result of concavity differences (higher θ will lead to higher k_s). Indeed, when normalised index values, k_{sn}, are calculated, the values for channels crossing inactive and active faults overlap.

Importantly, the channels crossing both constant-slip rate and inactive faults are much more similar to rivers that drain high but tectonically inactive topography than those crossing faults that have undergone a temporal variation in uplift rates: In Fig. 7, we show a selection of channels with similar headwater elevations, and identical lithologies (platform carbonates) to those in Fig. 6, but which do not cross any faults. Again, profile concavities lie in a comparable range ($0.44<\theta<0.66$); and for some of these rivers, normalised steepness indices are larger than those that cross active faults (e.g., N1). These findings are significant, because it is often assumed (either implicitly or explicitly) that continued uplift on a fault would likely result in any river crossing that structure showing some form of deviation from a concave-up 'equilibrium' profile (e.g. Kirby and Whipple, 2001; Hodges et al., 2004). However, the profiles in Figs. 5–7 strongly demonstrate that rivers crossing active normal faults do not *necessarily* have to show prominent profile convexities. In fact, they may adjust valley width or channel width instead of slope to keep pace with active uplift over million-year timescales (e.g. Whittaker et al., 2007b). Consequently, using long profiles alone to determine whether a fault is active/inactive is fundamentally flawed, as can be seen by comparing profile G1 crossing the Guarcino fault (now inactive) with S2 crossing the Cassino fault (active), and N2 (no fault) which have almost identical concavities, and similar steepness indices.

5.2. Comparison along strike on a single fault

Although the data on channels crossing faults with different temporal and spatial distributions of uplift credibly suggests that only rivers perturbed by an increase in fault throw rate within the last 1My have significant long-profile convexities, the quality of tectonic data in this area allows for an even stronger test of this hypothesis: comparison of river long profiles for channels along strike on the same fault. This approach is particularly robust because many valleys in the Apennines are normal-fault-bounded on just one side (Fig. 1), enabling us to compare (i) river response along the length of the fault with the spatial

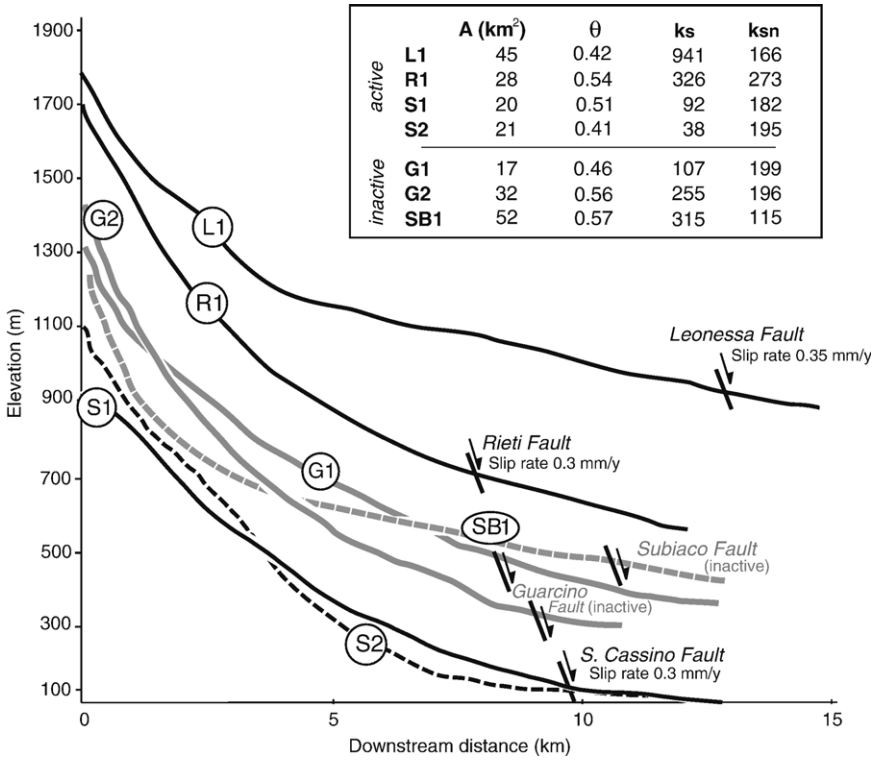

Fig. 6. Examples of channel long profiles crossing faults that have had a constant-slip rate for 3 My (black) or are now inactive (but were slipping for much of the Pleistocene (grey)). Locality numbers are shown geographically in Fig. 4. In the table, A is the drainage area, θ is the concavity, k_s is the steepness index and k_{sn} is the normalised steepness index assuming a reference θ of 0.5.

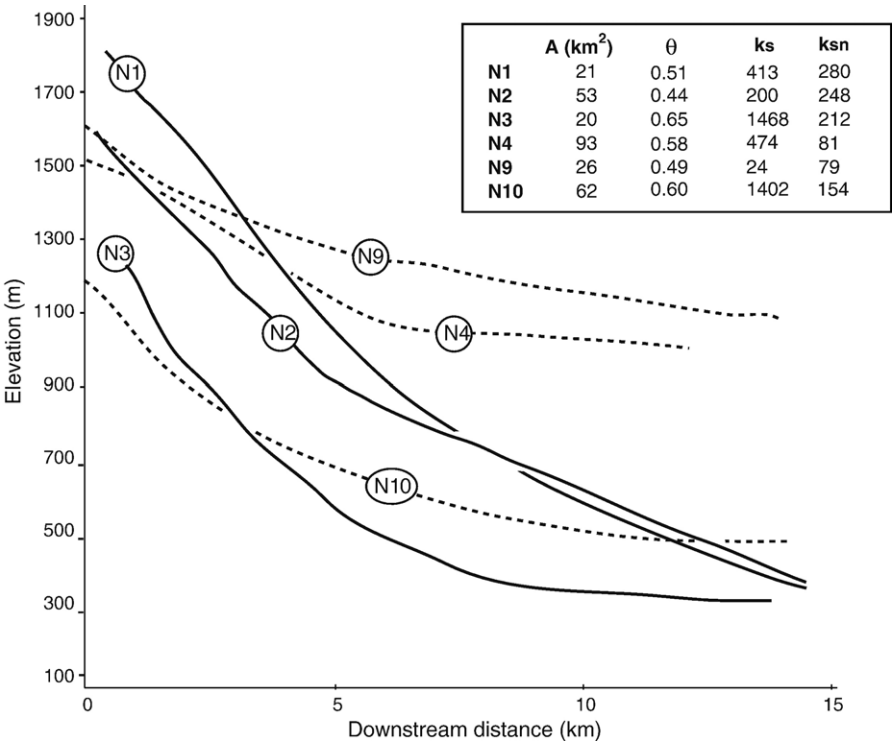

	A (km^2)	θ	ks	ksn
N1	21	0.51	413	280
N2	53	0.44	200	248
N3	20	0.65	1468	212
N4	93	0.58	474	81
N9	26	0.49	24	79
N10	62	0.60	1402	154

Fig. 7. Examples of channel long profiles draining high topography unbounded by active faults, with identical lithologies to the channels shown in Figs. 5 and 6. Locality numbers are shown geographically in Fig. 4. In the table, A is the drainage area, θ is the concavity, k_s is the steepness index, and k_{sn} is the normalised steepness index assuming a reference θ of 0.5.

distribution of uplift along strike (Fig. 2) and (ii) channel long profiles on the non-faulted margin of the valley that have experienced an identical regional base level history. Fig. 8 shows the Salto Valley, which is bounded to the NE by the 30 km long Fiamignano fault. The fault throw and throw rate distribution is a maximum in the centre of the fault, and dies out towards the tips (Figs. 3 and 8B(iii)). Currently, the maximum throw rate on the fault is ~1.1 mm/y (Roberts and Michetti, 2004; Whittaker et al., 2007b), but there is good evidence that it was slipping at ~0.3 mm/y prior to 1 Ma (Fig. 3) (c.f. Roberts and Michetti, 2004; Whittaker et al., 2007b). The fault has therefore undergone an increase in throw rate of a factor of 3–4 in the fault centre. The throw and throw rate declines towards the tips so these sections of the fault have undergone a smaller increase in slip rate. We document four rivers with drainage areas >10 km^2 crossing the fault (F2–F4 as shown previously, and F1 at the northeastern end of the fault), and four rivers on the other side of the valley (N5–N8) that do not cross any active structures. F1 and F4 lie near the tips of the fault, whilst F2 and F3 cross central segments (Fig. 8B (iii)). Again the rivers which do not cross the fault are characterised by concave profiles ($0.41<\theta<0.48$) and normalised steepness indices between 40 and 100 (Fig. 8B(i)) whilst those which cross the active fault show pronounced convex reaches in the long profiles of between 180 and 440 m in elevation, as measured upstream from the fault (Fig. 8B(ii)). The position of these convex reaches forms a roughly linear band behind the fault (Fig. 8B), and importantly, we note that the oversteepened reaches are largest on the two channels draining the central section of the fault, and smaller at the tips. They therefore appear to mirror the distribution of throw and throw rate along the fault (Fig. 8C(iii)). These observations also allow us to exclude the possibility that the convex reaches can be explained by base level fall, because the rivers on the southern side of the Salto Valley drain into the same axial channel (with the same base level history) but do not show these convex reaches. Moreover, rivers N5 and N6 (Fig. 8B(i)) offer us a good opportunity to calibrate the maximum effect that lithology could exert on river long profiles in this area. While river N5 flows entirely over sandstone with a Selby RMS of 40±5 (equivalent to a compressive strength of ≤50 MPa) (Selby, 1980) N6 also flows over Mesozoic carbonates in the upper part of the catchment with a Selby RMS of ~67±4 (compressive strength ~200 MPa). At this point, where the drainage area is ~10 km^2 we see the development of an oversteepened reach of ~100 m in elevation, measured from the lithological boundary. For rivers with larger drainage areas crossing lithological boundaries, we would expect the size of any convex reach to be less, as larger discharges tend to enhance erosivity, enabling the river to cope more effectively with the more resistant lithology (c.f. Stock and Montgomery, 1999). Consequently, for rivers considered in this study (i.e. those with $A>10$ km^2), an oversteepened reach of 100 m is likely to be the maximum that can be obtained for a lithological contrast between Miocene sandstone and Mesozoic limestones in this area. This is much smaller than the oversteepened reaches on the rivers crossing the Fiamignano fault on the other side of the valley, and thus supports the interpretation that the convex reaches on the NE flank are related to an increase in uplift rate on the Fiamignano fault rather than a lithological contrast.

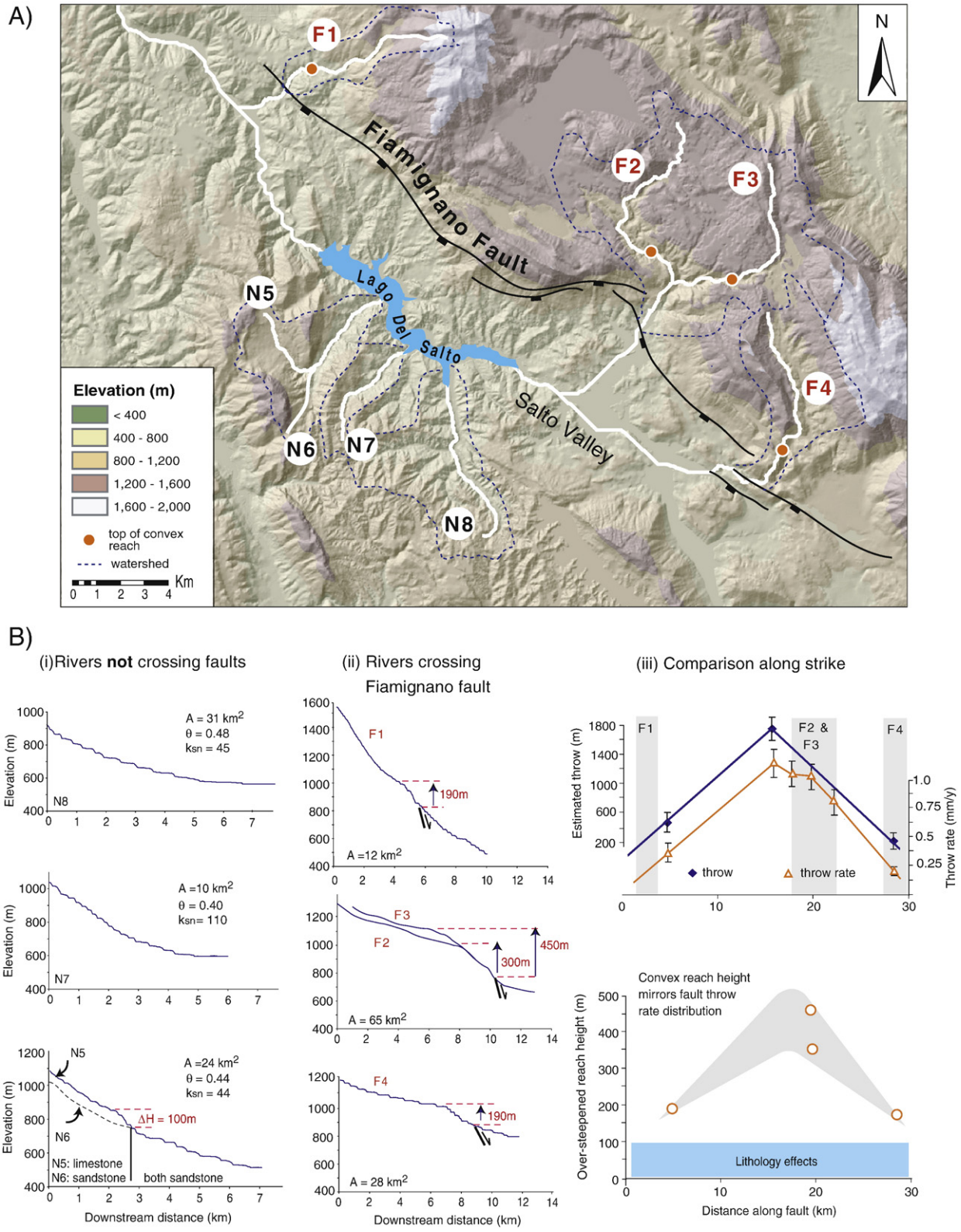

Fig. 8. (A) Detailed map of the Salto Valley and Fiamignano fault, showing rivers crossing the active normal fault (F1–F4) and rivers flowing on the other side of the valley (N5–N8). Dashed lines show catchment boundaries, and the red dots show the location of the tops of long-profile convexities. (B) Long profiles for rivers on (i) the SW side of the valley where there is no fault and (ii) the NE side of the valley, crossing the active fault, with the size of the convex reach, as measured from the fault. Panel (iii) shows the throw and throw rate distribution on the fault: this is mirrored by the spatial distribution of convex-reach heights.

6. Discussion

6.1. Explanations for convex reaches

Three main points can be drawn from the data presented in Sections 4 and 5:

(i) Rivers with drainage areas >10 km^2, crossing faults that have undergone an increase in fault uplift rate within the last million years, show the development of significant profile convexities.
(ii) Rivers crossing constant-slip rate or inactive faults do not show profile convexities, and have concavities and steepness indices comparable with rivers that do not cross active faults at all.
(iii) Our data show that these observations are not explained by appeal to lithology or base level change.

As we noted in Section 2, rivers with erosion dynamics approaching the detachment-limited end member will display concave-up long profiles at steady state (in the absence of major lithological variations) but are expected to develop long-profile convexities in response to an increase in relative uplift rate; i.e. as a *transient response* to the new tectonic forcing assuming that the river increases its erosivity through channel slope adjustment (Whipple and Tucker, 2002; Tucker and Whipple, 2002). In this case, the profile convexity propagates upstream as the catchment steepens in response to the new uplift rate, until the whole catchment eventually reaches a new steady-state topography. Previous work (Whittaker et al., 2007a,b) has already demonstrated that at least one river in this area (F3 — the Rio Torto) is definitely not in topographic steady state and is best explained as undergoing a transient response to tectonics. The generality of this explanation is therefore strengthened considerably by the fact that *all* the rivers crossing accelerated slip rate faults in the Central Apennines show similar profiles, whilst those crossing constant-slip rate faults do not. We therefore interpret the profiles in Figs. 5 and 8 as representing a transient response of detachment-limited river systems to an increase in tectonic uplift rates as a result of fault interaction within the last million years.

A significant challenge to this interpretation could be that while all the rivers crossing increased slip rate faults are detachment limited, all the rivers crossing constant-slip rate faults are better characterised by transport-limited erosion dynamics. However, we do not find this explanation persuasive. Field inspection of the rivers crossing the constant-slip rate faults show them to be indistinguishable from the channels crossing accelerated-rate faults, with bedrock exposed in the riverbed throughout. Gravel, where present, typically forms a thin veneer <0.5 m thick. Moreover, detailed grain-size analysis for rivers L1 and S1, presented in Whittaker et al. (2007b) shows that any sediment covering the bed would actually be fully mobilised at bankful flow conditions, and that derived Shields Stress estimates lie well above the transport-limited threshold (c.f. Mueller and Pitlick, 2005). The transport-limited end member is therefore inappropriate to describe erosional dynamics for L1 and S1, and a detailed comparison of the distribution of unit stream-power and footwall uplift along these channels supports the conclusion that they are likely to be in topographic steady state (c.f. Whittaker et al., 2007b). As these channels are typical of upland Apennine rivers, we consider these findings to be applicable generally.

These results are also significant because they help us to constrain the precise circumstances in which rivers near the detachment-limited end member develop profile convexities in this area, and how they evolve through time. Firstly, for lithology alone to be responsible for the significant convex reaches, drainage area would have to be very small, $\ll$10 km^2 or rock strength contrasts much bigger than 150 MPa. Moreover, for rivers responding to differential uplift rates >0.1 mm/y, channel slope adjustment is not the only way in which rivers could enhance their erosivity to keep pace with the imposed uplift (i.e., they can also narrow their channel width (Finnegan et al., 2005; Whittaker et al., 2007a) or their valley flat width (Whittaker et al., 2007b). Consequently, the fact that rivers crossing constant-slip rate faults do not show profile convexities, despite the uplift rate increasing towards the fault and the juxtaposition of rock types at this point, suggests that channel/valley adjustments must play an important role in enhancing fluvial erosivity. Such a valley width response has recently been documented for river S1 (Whittaker et al., 2007b). It therefore appears that the initial response of the rivers, at least in this area, to an increase in uplift rate is to steepen their channels, which is associated with channel narrowing (c.f., Duvall et al., 2004; Finnegan et al., 2005; Whittaker et al., 2007a). Through time, as the knickzone migrates upstream, channel slopes relax (c.f., Gasparini et al., 2006) with incision rates being matched by narrow valley and channel widths — note, for example, that for rivers FC1 and FC2 (Fig. 5A) the highest slopes are not at the fault although this is where the throw rate maximum lies.

The clear implication of the data presented here is that the response timescale of Apennine rivers to fault acceleration must be >1 million years, for these long-profile convexities to be retained generally in the landscape. A maximum response timescale of 3 million years is obtained by considering that the constant-slip rate faults now appear to have concave-up profiles and have apparently reached topographic steady state (Whittaker et al., 2007b). This is important because it suggests that transient long profiles retain tectonic information over periods >10^6 years and therefore provide a time-integrated archive of tectonic signals over this period. Below, we explore how this archive can be decoded to gain access to these tectonic signals.

6.2. Height of convex reaches as a function of uplift rate

The vertical height of a convex (oversteepened) reach upstream of an active fault is a measure that is easy to extract from DEM analysis, provided the position of the fault is either known from geological mapping, or can be identified from geomorphological considerations. Moreover, it is apparent from Fig. 5 that the size of long-profile convexities in the Central Apennines appears to be larger for rivers crossing faults with the highest present-day throw rates (and hence the largest

increase in uplift rates since 0.8 Ma). Additionally we note in Fig. 8 that the relative height of long-profile convexities for rivers crossing the Fiamignano fault also appears to mirror both the documented throw and throw rate on the fault. Because these knickzone heights (i) can be measured consistently throughout the field area as the fault traces are mapped at an excellent level of detail (Fig. 2; also Roberts and Michetti (2004)), and (ii) are evidently sensitive to tectonic forcing, we investigate, below, the extent to which river long-profile convexities record the magnitude of fault uplift rates.

Fig. 9 explicitly tests these ideas by plotting the height of all convex reaches (as measured from the fault/lithological boundary) on the rivers studied, as a function of both absolute throw rate as taken from the uplift rate profiles in Fig. 2, and also the calculated uplift rate increase (i.e. the difference in throw rates

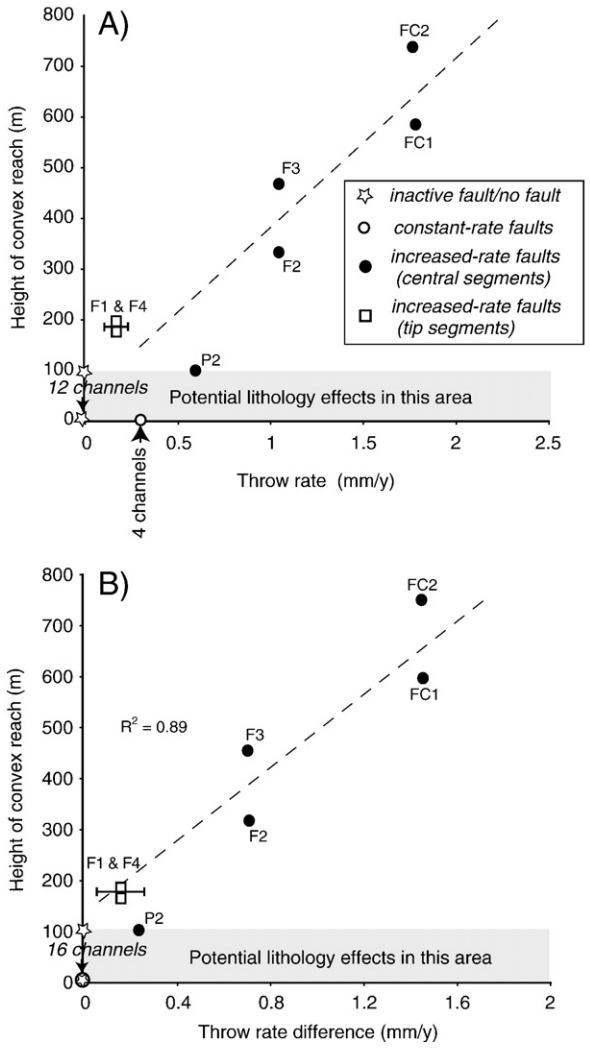

Fig. 9. Vertical height of long-profile convexities for rivers across the Central Apennines as a function of (A) fault uplift rate and (B) throw rate increase (i.e., the difference in throw rates before and after fault acceleration). The height of the convex reach is measured from the fault/lithological boundary to the upstream break in slope in the long profile. Dotted line represents the best-fit least-squares linear regression through the data and the alphanumeric letter codes refer to rivers shown in Figs. 4 and 8.

before and after the fault slip rate increase at 0.8 Ma; Fig. 9B). We estimate the throw rate increase by assuming fault segments have maintained similar length to their current mapped lengths (c.f. Cowie and Roberts, 2001) and that the distribution of throw rates along strike prior to acceleration mirrored the documented distribution of throw rates on the constant-slip rate faults (i.e. a maximum of ~0.35 mm/y that declines towards the tips, as illustrated for many of the faults in Fig. 2). Fig. 9B shows oversteepened reach height as a function of current slip rates; the grey bar illustrates that knickzones of <100 m elevation can be potentially explained by lithological differences. Although faults with higher present-day rates of displacement do have larger long-profile convexities (Fig. 9B), it is instructive to note that rivers located toward the ends of the increased slip rate faults actually have significant profile convexities despite having lower absolute throw rates than either the constant rate examples (where there are no oversteepened reaches) or the Pescasseroli case (P), where the documented slip rate is approximately twice as large (0.55–0.6 mm/y). This confirms that the absolute slip rate is not an ideal predictor of convex-reach height. However, if we present the results in terms of a slip rate increase (Fig. 9B), we produce a considerably more linear trend. Firstly, all the channels that cross constant-slip/inactive faults, or do not cross faults at all plot at the origin, apart from the 100 m (lithological) convexity on channel N5 (Fig. 8B). In contrast, the convex-reach heights on the centrally-located fault segments lie on an array with increasing degree of slip rate increase. Overall, for a doubling in size of the throw rate difference, the height of the knickzone generated appears to increase by a factor of ~2. This result is exciting because it is a graphic illustration of the way in which transient landscapes directly record tectonic signals and shows the predictive power of this approach. Moreover, the data suggest strongly that the degree to which the fluvial system is *perturbed* from its initial conditions is vital in determining the magnitude of the transient response to tectonics.

To understand this relationship, with the aim of making generally applicable, quantitative predictions of tectonic forcing from the magnitude of long-profile convexities, we need to understand the physical generation of convex reaches upstream of faults that have undergone an increase in uplift rate. For detachment-limited channels, or for rivers approaching this end member, long-profile convexities are produced by the disparity in wavelength between the 'new' uplift field, and the length scale over which the channel is able to increase its erosivity in response to this (Tucker and Whipple, 2002; Whittaker et al., 2007b). If we consider for simplicity the end member case where the oversteepened reach remains at the fault (i.e. no river response) then the height of the convex reach would simply represent the accumulation of relative footwall uplift on the fault since the acceleration event. In this case, the size of the profile convexity should scale as the difference in uplift rate between the 'original' and 'new' throw rates, minus any hangingwall aggradation, and multiplied by the time available. For example an imbalance between uplift and erosion rates of 0.1–0.2 mm/y could produce an oversteepened reach height of ~100–200 m over the past 1 Ma. This is roughly the correct order of

magnitude for convexities on the rivers crossing the lower slip rate faults (e.g., Pescasseroli, and ends of Fiamignano). However, because the increased rate of uplift acts to steepen the channel near the fault, increasing local fluvial incision rates until the rate of downcutting balances the uplift field, the resulting knickzone will propagate back up the catchment as a wave as the erosion rates within the convex reach are much greater than those above it (Whipple and Tucker, 2002; Gasparini et al., 2006). Consequently, the size of the convex reach, as measured from the fault, is a function not only of the magnitude of the perturbation signal but also the speed at which the knickzone migrates up the profile, and the relative distribution of uplift in the (back-tilted) footwall.

6.3. Comparison with model outcomes

To investigate tectonic controls on knickzone generation and migration explicitly, we use the CHILD landscape evolution model (Tucker et al., 2001) to simulate how convex reaches may develop and grow with time for rivers crossing active normal faults in the Apennines. We use a detachment-limited erosion law to model a river incising across a back-tilted footwall: i.e., a maximum in uplift rate at the fault, with a linear decline in uplift rate to a fulcrum located at 10 km behind the fault. The fulcrum position has been chosen to reflect the average fault spacing in the Central Apennines (c.f. Roberts and Michetti, 2004). A full description of the model setup and parameters used can be found in the Appendix (see also Attal et al., in press). We emphasize that the aim of this modelling is not to reproduce the specific long-profile development of any one river in the Central Apennines, which would clearly require a detailed knowledge of hangingwall base level history and the precise distribution of footwall uplift for each catchment (c.f. Whittaker et al., 2007b). Instead, we aim to test whether the signature we have documented in Fig. 9 (i.e. that convex-reach heights scale with an increase in fault uplift rate) is broadly consistent with the behaviour one might expect for rivers near a detachment-limited end member that are perturbed by an increase in fault uplift rate.

In Fig. 10A, we take an initial steady-state profile that is in topographic steady state with respect to an uplift rate of 0.3 mm/y and instantaneously increase the uplift rate to 1 mm/y. Consistent with the work of Whipple and Tucker (2002), an oversteepened reach develops that reflects the imbalance of the 'new' tectonic uplift field, and the channel's ability to incise. Over time, the knickzone migrates upstream (with a velocity a function of the celerity of the wave of incision — Section 6.4; see also Tucker and Whipple, 2002). The break in slope at the top of the convex reach separates the part of the channel that is adjusting to the new uplift field from the part that is yet to detect the throw rate increase. Importantly, by 0.5–0.75 Ma, an oversteepened reach of ~400–600 m has developed in our model setup, similar to the size of convex reaches seen on rivers crossing the central sections of high slip rate faults in the Apennines (e.g. rivers FC1,2 and F2, F3). Moreover, if we consider rivers responding to different uplift rate increases over an identical time period (Fig. 10B), here modelled to be 0.5 My, we

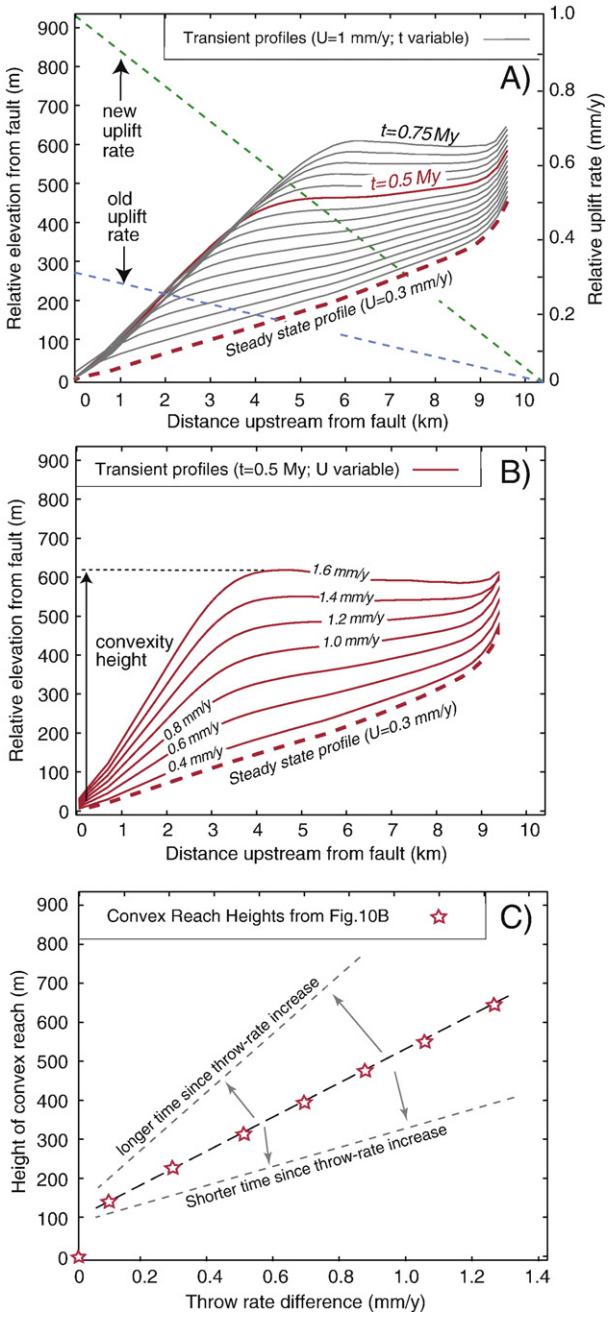

Fig. 10. (A) Long profile evolution, for a river crossing a fault (located at 0 km) that undergoes an increase in uplift rate. Initial long profile (red dashes) is in steady state with the initial throw rate (0.3 mm/y at fault), with a linear declines upstream (blue dashes). Throw rate is instantaneously increased to 1 mm/y at fault (green dashes). Grey lines show transient profiles in 0.05 My time-steps. Red line shows profile at t=0.5 My, identical to "1 mm/y" long-profile in Fig. 10B. The part of the profile downstream of the break in slope is approximately re-equilibrated with respect to the new uplift field. (B) Long profiles evolved at 0.5 My for a range of 'new' uplift rates, using identical starting conditions to (A). Arrow illustrates convex-reach height after 0.5 My at a throw rate of 1.6 mm/y. (C) Height of profile convexities (measured from fault to slope break) at 0.5 My in (B), as a function of the throw rate increase. Arrows in (C) show schematically how distribution of convex-reach heights would vary for shorter/longer model run times.

do generate larger oversteepened reaches as the 'new' throw rate grows in magnitude. The height of these convex reaches is clearly a function of the difference in throw rate between the 'old' and the 'new' rates (compare Figs. 10C with 9). Moreover, this modelling work allows us to predict that the slope of the fit between convex-reach height and throw rate increase is itself a function of the time since the slip rate increase occurred (shown schematically in Fig. 10C). For 'real' channels drainage area exerts an additional control on knickzone retreat rate, and the upstream distribution of A may differ between catchments (see Section 6.4). We also note that the heights of the convex reaches generated in these model runs are similar to those documented in Fig. 9, although the timescale is somewhat shorter (0.5 My). However, these model runs do not take into account any hangingwall sedimentation, which is clearly evidenced, for example, in the Fucino basin (Fig. 3B), and which would reduce the relative size of long-profile convexities on rivers FC1 and FC2 (essentially by reducing the relative uplift rate change experienced by the river). These field and modelling results are exciting because they demonstrate that transient river responses to a change in fault uplift rate, in the form of long-profile convexities, act as a 'tape recorder' of tectonic signals over million-year timescales. This raises the prospect that uplift rate information could be extracted from tectonically perturbed landscapes without having to assume the landscape has reached topographic steady state, particularly in areas where, e.g., fault slip rates are poorly known but initiation ages are well documented.

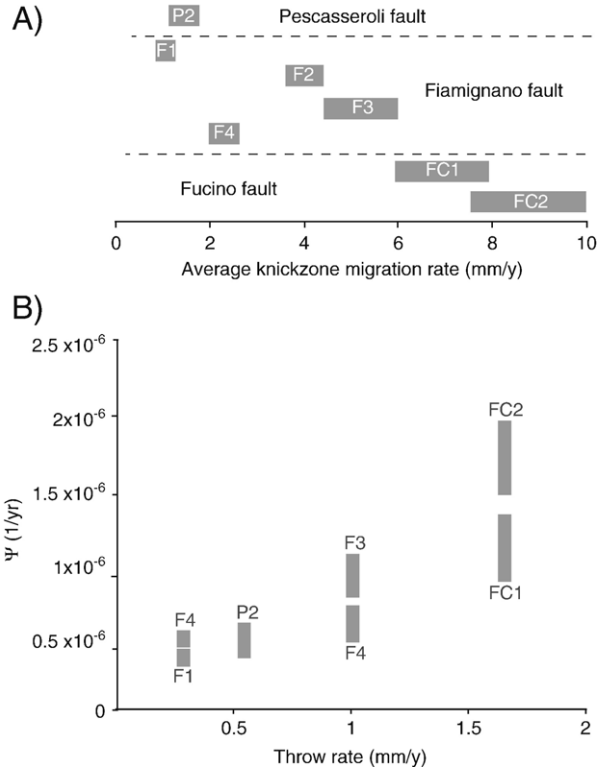

Fig. 11. (A) Knickzone migration rate, V, for rivers crossing faults in the Apennines (B) Variation of the constant Ψ in the expression $V = \Psi\sqrt{A_{f(L)}}$ with slip rate for different faults.

6.4. Knickzone migration rates

The data presented in this paper also give us a unique opportunity to quantify the long-term migration rate of long-profile convexities, for river systems near the detachment-limited end member and crossing carbonate bedrock. If we take the top of the convex reach in each of the long profiles to represent the distance upstream the effects of the fault throw rate increase has propagated (c.f. Whittaker et al., 2007b), then we can estimate the mean rate of knickzone migration for each of the rivers (Fig. 11A — grey bars show the range of propagation estimates assuming the increase in slip rate occurred between 0.75 and 1 Ma). In general, rates vary by one order of magnitude from 1 mm/y to 10 mm/y, within the range predicted by other workers (e.g. Weissel and Seidl, 1998; Dorsey and Roering, 2006), although we note that the fastest rates of knickzone propagation are for rivers crossing the Fucino fault, which has the greatest present-day slip rate (>1.5 mm/y where rivers FC1 and FC2 cross) and hence also the greatest degree of fault acceleration. Theoretically, knickzone retreat can also be enhanced by softer rock types, and by greater catchment discharge (Tucker and Whipple, 2002). Lithology contrast is unlikely to be a satisfactory explanation, as all the rivers presented here cross identical bedrock, with no significant differences documented in Selby rock mass strength (typical compressive strength of ≤200 MPa). However, drainage areas do vary by a factor of three between the catchments.

The velocity of knickzone retreat, V, should scale with the wave celerity for any detachment-limited erosion law. For a unit stream-power model (i.e. $m=0.5$, $n=1$ in Eq. (1)), V should (all other factors being equal) be a function of the square root of discharge and therefore drainage area, $\sqrt{A}$ (Tucker and Whipple, 2002). We therefore explicitly evaluate whether this effect accounts for the differences in knickzone migration rate documented here: To do this, we iteratively calculate knickzone retreat rate as a function of changing drainage area with downstream distance, $\sqrt{A_{f(L)}}$:

$$V = \Psi\sqrt{A_{f(L)}} \tag{3}$$

and estimate the value of the constant Ψ that reproduces the current position of the oversteepened reach top, L_k for each channel according to

$$L_k = L_f - \left(\Psi\sqrt{A_{f(L)}}\right)t \tag{4}$$

where L_f is the downstream position of the fault, and t is the time period (in this instance 0.75–1 Ma). Explicit in this formulation is the notion that the knickzone will migrate progressively more slowly upstream as the drainage area grows smaller. If drainage area is the main control on knickzone migration rate, then we expect Ψ to be roughly similar between the channels.

However, as can be seen in Fig. 11B, Ψ is a function of fault slip rate, with values rising from $<3\times10^{-7}$ y^{-1} for low slip rate

faults to $>2\times10^{-6}$ y^{-1} for higher slip rate segments. For a standard drainage area of 20 km^2, this value would imply oversteepened reach propagation rates of between 2 and 8 mm/y, emphasising that fault throw rates have a significant effect on the velocity of knickzone propagation. In fact, the convex-reach migration rate for rivers crossing active faults is typically five times the fault slip rate in this setting, e.g. Fucino fault has a throw rate of 1.5–2 mm/y and the long-profile convexity has migrated up the channel at a rate of 6–10 mm/y (Fig. 11A).

Importantly, the relationship between faster propagation rates and the degree of tectonic perturbation can be explained if Ψ is also controlled by channel slope. A larger imbalance between 'old' and 'new' uplift rates on the fault leads to the accumulation of more slip per unit time and the generation of a steeper knickzone at the fault. If the knickzone retreat rate (the wave celerity) is a positive function of channel gradient (Tucker and Whipple, 2002) then the profile convexity reach will migrate more rapidly. This applies where $n>1$ for a strictly detachment-limited stream-power erosion law Eq. (1) and has also been demonstrated to fit the pattern of knickpoint evolution in Eastern Australia (Weissel and Seidl, 1998). However, values of n substantially bigger than 1 can be physically difficult to explain, or imply erosion processes such as cavitation that we have not observed (Whipple et al., 2000). However, this effect could also be generated by an erosion threshold (c.f. Snyder et al., 2003) that is exceeded more readily for higher channel slopes, or an explicit role for sediment in increasing erosion rates near the fault (c.f. Gasparini et al., 2006). i.e., although the rivers can be adequately described by a detachment-limited model, in detail, they do not quite lie at this end member (c.f. Cowie et al., in press). Furthermore, as both the height of the 'potential' oversteepened reach (i.e. the knickzone pinned at the fault) and the rate at which the convexity propagates upstream are both functions of the magnitude of the tectonic perturbation, this explains why the heights of convex reaches in the Apennines scale so convincingly with the degree of fault acceleration.

6.5. Transient fluvial geomorphology as a tool for extracting tectonic information; the danger of assuming topographic steady state

The data presented in this paper show that transient long profiles can be used to make sophisticated interpretations of fault uplift rates for time periods >1 My. However, rivers in the Central Apennines also provide a clear illustration of the potential problems associated with trying to extract tectonic information from fluvial geomorphology. In particular, we stress that our interpretations rest fundamentally on the identification of river channels as being transient rather than in topographic steady state. In fact, the data sets presented here could be misinterpreted if one approached tectonic geomorphology solely from the perspective of normalised steepness indices, where higher values are typically assumed to imply greater rates of rock uplift (c.f. Kirby et al., 2003; Wobus et al., 2006). Difficulties arise both in principle and in practice. Firstly, in slope-area space, it is difficult to distinguish a river undergoing a transient response to tectonics or base level fall, from one which is actually in topographic steady state, but which flows from a zone of lower uplift (characterised by lower values of k_{sn}) to a zone of higher uplift (and larger k_{sn}). Both would be characterised by a convex reach in the long profile and a spike in a slope-area plot, illustrated for the (transient) river F3 (Fig. 12A,B). However, a straightforward application of steady-state paradigms to interpret F3 would predict an uplift field that is significantly displaced relative to the real tectonic situation (Fig. 12C). These problems are clearly recognised by Wobus et al. (2006), and they argued that in these circumstances the plan view map location of profile convexities is the key discriminant: transient knickzones, caused by base level fall or uplift change should appear at an approximately constant elevation around a drainage basin, representing the constant vertical propagation rate of the oversteepened reach throughout the catchment. In contrast, convex reaches separating two regions in steady state with respect to their (differing) uplift fields, would tend to have a spatially linear distribution (Fig. 3 in Wobus et al., 2006).

Unfortunately, in practice this can be difficult to apply. On the broad scale, the long-profile convexities identified in this study form approximately linear trends, because they are generated from linear fault structures (Fig. 12D). Moreover, because evolution of the fault array fundamentally controls the long-term development of these drainage networks (c.f. Cowie et al., 2006), it is probably unwise to view these tectonic perturbations as being super-imposed onto an existing drainage structure; in the Italian examples, fault growth has led to the development of axial rivers flowing parallel to the fault, with shorter rivers periodically cutting across the fault block. The result in the Apennines is that, in map view, the zones of high steepness index ("high uplift") and low-steepness index ("low uplift") do not correlate in a simple way with the real uplift field on the faults — here illustrated for the Fiamignano fault, where the zone of high k_{sn} largely covers the hangingwall of the fault (Fig 12C,D). Of course, to calculate robust steepness indices one ideally needs to cover one to two orders of magnitude in drainage area. However, in many of the Italian examples, the entire knickzone upstream of the fault occurs within one order of magnitude in A, so the method is not particularly sensitive to tectonic signals on the length scale of a normal-fault block.

Consequently, while the use of normalised steepness indices have proven to be informative when considering larger channels on a regional scale (e.g. Wobus et al., 2003), our experience here suggests that widespread use of such an approach is likely to be inappropriate (i) for channels with $A<100$ km^2 (ii) in extensional settings where the fault spacing is small (i.e., <10–15 km) and (iii) without independent data that validate steady-state assumptions. Diagnostic signatures of detachment-influenced fluvial systems undergoing a transient response to tectonics (in addition to long-profile convexities) include small-wavelength spikes in unit stream power that do not correlate with lithology or the likely distribution of uplift, channel widths that are decoupled from drainage area, narrowed valley widths, and hillslopes rejuvenated to the angle of repose within the convex reach (Whittaker et al., 2007b). In the presence of one or more of these key features, we argue that inferences about tectonics drawn from geomorphic studies that

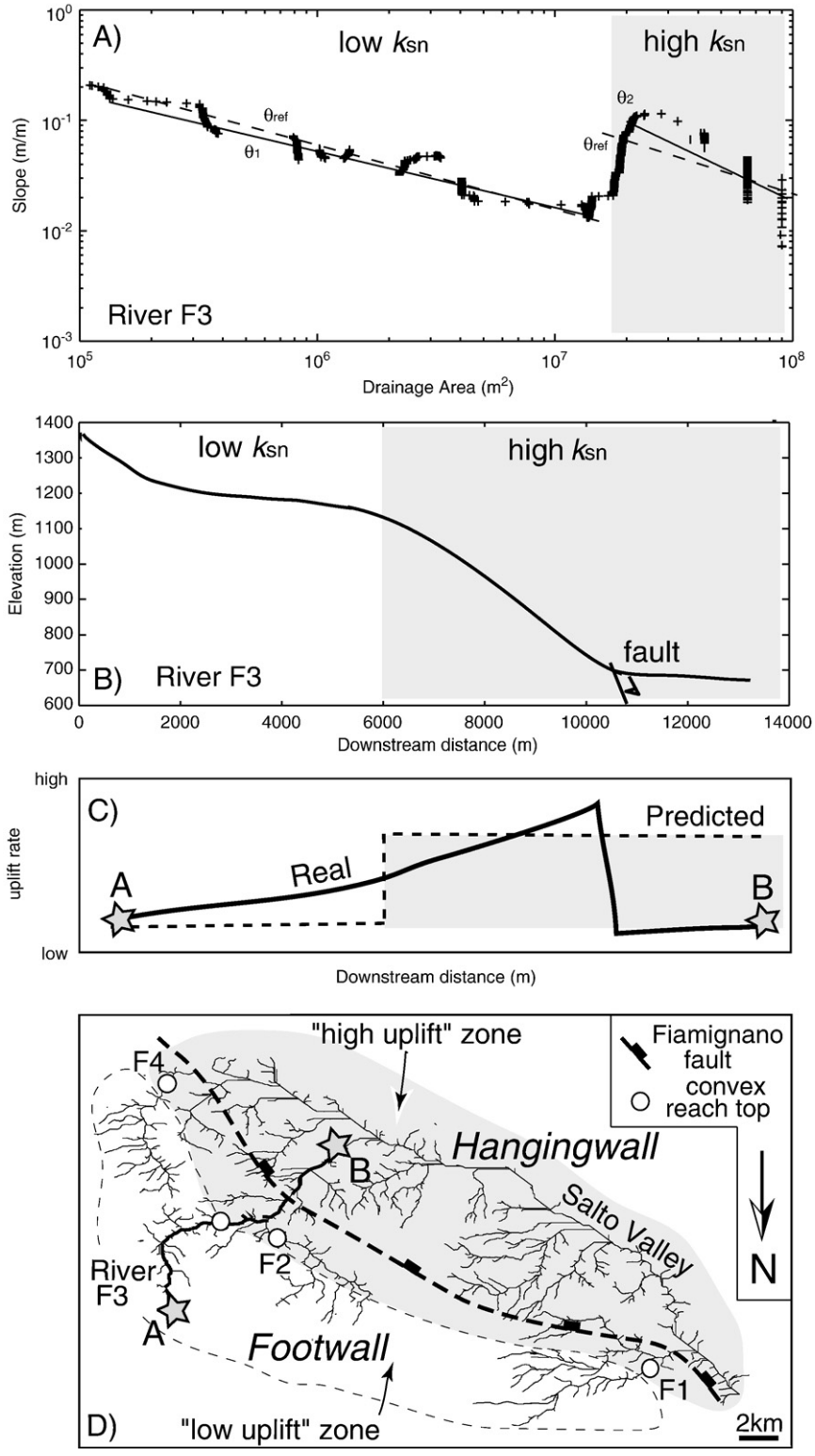

Fig. 12. (A) Slope-area plot for river F3 showing low and high steepness index (k_{sn}) zones. θ_1 and θ_2 are the profile concavities (0.5 and 0.7, respectively), and θ_{ref} is an average reference concavity for the region. (B) River long profile showing zones of high and low k_{sn} derived from (A). (C) Relative uplift rates in reality (thick line) and erroneously predicted by comparing steady-state normalised steepness indices (dashed line). Stars show profile location on plan view map below. (D) Plan view pattern of uplift distribution if steady state is assumed, compared with real distribution for the Fiamignano fault (dashed line) bordering the Salto Valley (c.f. Fig. 8; north is reversed here). The zone of predicted 'high' uplift largely covers the hangingwall of the fault. Convex-reach tops (circles) are shown for other rivers crossing the fault (rivers F1, F2, F4).

assume that the rate of rock uplift equals the rate of fluvial erosion run the risk of producing misleading conclusions.

7. Conclusions

Although there has been considerable focus in recent years on using transient landscapes to parameterise river erosion laws (Tomkin et al., 2003; Van der Beek and Bishop, 2003), comparatively little attention has been paid to the potential to extract tectonic signals from fluvial systems that are not in topographic steady state. To some extent, this is surprising because it is widely recognised that transient responses to tectonic forcing potentially contain more diagnostic information about boundary conditions than landscapes at steady state (Tucker and Whipple, 2002; Whipple and Tucker, 2002). However, a significant problem to date has been a lack of well-calibrated field examples of fluvial systems exposed to a range of tectonic uplift rates in both temporal and spatial domains. This paper has addressed this outstanding challenge using an active normal-fault system in the Central Apennines of Italy, where unique constraints exist on fault uplift rates through time and where transient river responses have already been documented in individual catchments (Whittaker et al., 2007a,b).

By comparing 15 large rivers crossing active and inactive normal faults, with 10 rivers not crossing any faults, we show firstly that channels with drainage area >10 km^2 and crossing faults that have undergone an increase in uplift rate within the last million years are characterised by significant long-profile convexities. In contrast, rivers crossing constant-slip rate faults have concave-up profiles with similar concavities and steepness indices to rivers crossing inactive faults and tectonically quiescent areas. We show that these convexities cannot be explained by base level or lithological effects, and consequently, the convex reaches are best explained as the transient response of a detachment-limited river system to an increase in fault uplift rate. We demonstrate that the height of the convex reaches scales with the magnitude of the slip rate increase on the faults and that this signal is consistent between faults with different uplift rates and also with along-strike variations in slip rate for a single fault segment. Reach height is controlled by (i) the magnitude and distribution of uplift rate in the footwall, (ii) the rate at which the convex reach (the knickzone) migrates up the profile and is mediated by any sediment accumulation in the adjacent hangingwall basin. Using the CHILD landscape model, we demonstrate that these findings are consistent with the behaviour, over 0.5–0.75 My time periods, of detachment-limited rivers crossing back-tilting normal faults. The results thus raise the prospect of using long-profile convexities to decode temporal variations in tectonic uplift rates in other transient settings. Additionally, we show that field estimates of knickzone propagation rates are a function of fault slip rate as well as drainage area, with velocities varying from <2 mm/y to >8 mm/y for a reference drainage area of 20 km^2. This result requires that the slope exponent n for a detachment-limited stream-power erosion law to be >1 (i.e. faster propagation on steeper slopes), but could also be explained either by an erosion threshold or an explicit role for sediment in setting erosion rates such that the channels are close, but not quite at the detachment-limited end member.

The results in this study are important because they show that transient landscapes act as an archive of past tectonic events over million-year timescales. In particular, channels perturbed by active faulting have convex reaches in their long profiles that can be used as an explicit proxy for uplift rate. However, we demonstrate that geomorphic analyses which assume topographic steady state could give misleading results in extensional settings, particularly on the scale of an individual fault block. We therefore underline the importance of establishing the extent of transience in a landscape as an important precursor to any attempt to extract tectonic signals from geomorphic data.

Acknowledgements

This work was supported by NERC Research Grants NER/S/A/2002/10359 (Whittaker), NE/B504165/1 (Cowie, Roberts, Attal, Tucker), and ARO Grant 47033EV (Tucker). We thank Zana Conway and Richard Granville for their help in collecting field data and Eutizio Vittori for supplying the DEM. We are grateful to two anonymous reviewers for their positive reviews.

Appendix A: Model setup

We use the Channel-Hillslope Integrated Landscape Development (CHILD) model (Tucker et al., 2001) to model the evolution of rivers draining the footwalls of extensional faults in the Central Apennines of Italy (c.f., Attal et al., in press). The tectonic setup is a back-tilted footwall characterised by an uplift field that decreases linearly (in a direction perpendicular to the fault) to the fulcrum located 10 km into the footwall; this is consistent with average fault spacing, and 'domino' fault-block tilting found in the Central Apennines (c.f. Roberts and Michetti, 2004). The parameters used in the model are described in Table A1, and are scaled to approximately emulate a typical catchment draining the footwall of an active normal fault in this part of Italy (e.g., the Rio Torto, Whittaker et al., 2007a). A full description can be found in Attal et al. (in press).

A detachment-limited fluvial incision law is used within the CHILD model. The initial long profile (t=0), is in steady state with a fault throw rate of 0.3 mm/y The throw rate is then raised to different values and the response of the river's long profile is displayed in Fig. 10. The erosion rate of the channel, E, is computed as follows:

$$E = k_b \tau^p \tag{A1}$$

where k_b is the erodability coefficient, τ is the fluvial shear stress and p is an exponent >0.

$$\tau = k_t (Q_c/W)^m S^n \tag{A2}$$

where k_t is the shear stress coefficient, Q_c is the discharge, W is the channel width, and m, n are positive exponents. Manning's equation is used to model roughness, i.e.

$$k_t = \rho g \cdot n_m^{3/5} \tag{A3}$$

where ρ is the fluid density, g represents gravitational acceleration, and n_m is Manning's roughness coefficient. Combining Eqs. (A1)–(A3) gives

$$E = k_b k_t^p (Q_c/W)^{m \cdot p} S^{n \cdot p} = K(Q_c/W)^{m \cdot p} S^{n \cdot p} \quad \text{(A4)}$$

which can be written as

$$E = K(Q_c/W)^{0.9} S^{1.05} \quad \text{(A5)}$$

when appropriate numerical values are used (see Table A1). Channel width is described by Finnegan et al.'s (2005) equation, which allows width to narrow in regions of high slope.

$$W = k_{\mathrm{wf}} Q_c^{3/8} S^{-3/16} \quad \text{(A6)}$$

This has been shown to be a better approximation to real channel widths than conventional hydraulic scaling for rivers in Italy undergoing a transient response to tectonic forcing (Whittaker et al., 2007a).

Table A1
Parameters used in the landscape model

Parameter	Value
Catchment's drainage area, A_c	~65 km^2
Mean precipitation rate, P	0.75 mm/h
Storm duration T_r	22 h
Inter-storm duration T_b	260 h
Mean discharge at the outlet, Q_c	13.6 m^3/s
Erodability coefficient k_b	8.10^{-6} m$^{-1/2}$kg$^{-3/2}$ s^2
Shear stress coefficient k_t	1000 kg m^{-2} s^{-2}
Manning's roughness coefficient n_m	0.025
Channel width coefficient k_{wf}	3.2 m$^{-1/8}$ s$^{3/8}$
Exponents: m, n, p	0.6, 0.7, 1.5

References

Accordi, G., Carbone, F., Civitelli, G., Corda, L., De Rita, D., Esu, D., Funicello, R., Kotsakis, T., Mariotti, G., Sposato, A., 1986. Lithofacies map of Latium-Abruzzo and Neighbouring areas. Consiglio Nazionale delle Ricerche, Italy.

Anders, A.M., Roe, G.H., Hallet, B., Montgomery, D.R., Finnegan, N.J., Putkonen, J., 2006. Spatial patterns of precipitation in the Himalaya. In: Willet, S., Hovius, N., Brandon, M., Fisher, D. (Eds.), Tectonics, climate and landscape evolution. GSA special paper, vol. 398, pp. 55–74.

Attal, M., Tucker, G.E., Whittaker, A.C., Cowie, P.A., Roberts, G.P., in press. Modelling fluvial incision and transient landscape evolution: influence of dynamic channel adjustment, Journal of Geophysical Research.

Bosi, C., Messina, P., 1991. Ipotesi di correlazione fra successioni morfolitos-tratigrafiche plio-pleistoceniche nell'Appennino lazialeabruzzese, Studi Geologici Camerti. Special Volume CROP 11, 257–263.

Burbank, D.W., Anderson, R.S., 2001. Tectonic Geomorphology. Blackwell Science, London. 274 pp.

Cavinato, G.P., 1993. Recent tectonic evolution of the Quaternary deposits of the Rieti Basin (Central Apennines, Italy): southern part. Geologica Romana 29, 411–434.

Cavinato, G.P., De Celles, P.G., 1999. Extensional basins in tectonically bimodal central Apennines fold-thrust belt, Italy: response to corner flow above a subducting slab in retrograde motion. Geology 27, 955–958.

Cavinato, G.P., Carusi, C., Dall'Asta, M., Miccadei, E., Piacentini, T., 2002. Sedimentary and tectonic evolution of Plio-Pleistocene alluvial and lacustrine deposits of Fucino Basin (central Italy). Sedimentary Geology 148, 29–59.

Centamore, E., Nisio, S., 2003. Effects of uplift and tilting in the central-northern Apennines, Italy. Quaternary International 101–102, 93–101.

Cowie, P.A., Attal, M., Tucker, G.E., Whittaker, A.C., Naylor, M., Ganas, A., Roberts, G.P., 2006. Investigating the surface process response to fault interaction and linkage using a numerical modeling approach. Basin Research 18, 231–266.

Cowie, P.A., Whittaker, A.C., Attal, M., Tucker, G.E., Roberts, G.P., Ganas, A., in press. New constraints on sediment-flux dependent river incision: implications for extracting tectonic signals from river profiles. Geology.

Cowie, P.A., Roberts, G.P., 2001. Constraining slip rates and spacings for active normal faults. Journal of Structural Geology, 23, 1901–1915.

D'Agostino, N., Jackson, J.A., 1999. Convective support of long-wavelength topography in the Apennines (Italy). Terra Nova, 11, 234–238.

D'Agostino, N., Jackson, J.A., Dramis, F., Funiciello, R., 2001. Interactions between mantle upwelling, drainage evolution and active normal faulting: an example from the central Apennines (Italy). Geophysical Journal International 147, 475–497.

Dadson, S.J., Hovius, N., Chen, H., Dade, W.B., Hsieh, M., Willett, S.D., Hu, J., Horng, J., Chen, M., Stark, C.P., Lague, D., Lin, J., 2003. Links between erosion, runoff variability and seismicity in the Taiwan orogen. Nature 426, 648–651.

Dorsey, R.J., Roering, J.J., 2006. Quaternary landscape evolution in the San Jacinto fault zone, Peninsular Ranges of Southern California: transient response to strike-slip fault initiation. Geomorphology 73, 16–32.

Duvall, A., Kirby, E., Burbank, D.W., 2004. Tectonic and lithologic controls on channel profiles and processes in coastal California. Journal of Geophyicical Research 109 (F3). doi:10.1029/2003JF000086.

Finlayson, D.P., Montgomery, D.R., Hallet, B., 2002. Spatial co-incidence of rapid inferred erosion with your metamorphic massifs in the Himalayas. Geology 30, 219–222.

Finnegan, N.J., Roe, G., Montgomery, D.R., Hallet, B., 2005. Controls on the channel width of rivers: implications for modelling fluvial incision of bedrock. Geology 33, 229–232.

Gasparini, N.M., Bras, R.L., Whipple, K.X., 2006. Numerical modelling of non-steady state river profile evolution using a sediment-flux-dependent incision model. In: Willet, S., Hovius, N., Brandon, M., Fisher, D. (Eds.), Tectonics, climate and landscape evolution. GSA special paper, vol. 398, pp. 127–141.

Giraudi, C., Frezzotti, M., 1997. Late Pleistocene glacial events in the Central Apennines, Italy. Quaternary Research 48, 280–290.

Hack, J.T., 1957. Studies of longitudinal profiles in Virginia and Maryland. U.S. Geological Survey Professional Paper. 249B.

Hodges, K.V., Wobus, C., Ruhl, K., Schildgen, T., Whipple, K., 2004. Quaternary deformation, river steepening, and heavy precipitation at the front of the Higher Himalayan ranges. Earth and Planetary Science Letters 220, 379–389.

Howard, A.D., Kerby, G., 1983. Channel changes in badlands. Geological Society of America Bulletin 94, 739–752.

Howard, A.D., Dietrich, W.E., Seidl, M.A., 1994. Modelling fluvial erosion on regional to continental scales. Journal of Geophysical Research 99, 13971–13986.

Hunstad, I., Selvaggi, G., D'Agostino, N., England, P., Clarke, P., Pierozzi, M., 2003. Geodetic strain in peninsular Italy between 1875 and 2001. Geophysical Research Letters 30 (4), 1181. doi:10.1029/2002GL016447.

Hurtrez, J.-E., Lucazeau, F., Lavé, J., Avouac, J.-P., 1999. Investigation of the relationships between basin morphology, tectonic uplift, and denudation from the study of an active fold belt in the Siwalik Hills, central Nepal. Journal of Geophysical Research 104 (B6), 12779–12796.

Kirby, E., Whipple, K.X., 2001. Quantifying differential rock-uplift rates via stream profile analysis. Geological Society of America Bulletin 29, 415–418.

Kirby, E., Whipple, K.X., Tang, W., Chen, Z., 2003. Distribution of active rock uplift along the eastern margin of the Tibetan Plateau: inferences from bedrock channel longitudinal profiles. Journal of Geophysical Research 108 (B4), 2217. doi:10.1029/2001JB000861.

Lague, D., Davy, P., 2003. Constraints on the long term colluvial erosion law by analysing slope-area relationships at various tectonic uplift rates in the Siwalik Hills (Nepal). Journal of Geophysical Research 108, 2129. doi:10.1029/2002JB001893.

Lavé, J., Avouac, J.-P., 2001. Fluvial incision and tectonic uplift across the Himalayas of central Nepal. Journal of Geophysical Research 106, 26561–26591.

Lavecchia, G., Brozzetti, F., Barchi, M., Menichetti, M., Keller, J.V.A., 1994. Seismotectonic zoning in east-central Italy deduced from an analysis of the

Neogene to present deformations and related stress fields. Geological Society of America Bulletin, 106, 1107–1120.
Merrits, D.J., Vincent, K.R., 1989. Geomorphic response of coastal streams to low, intermediate and high rates of uplift, Mendocino triple junction region, northern California. Geological Society of America Bulletin 101, 1372–1388.
Michetti, A.M., Brunamonte, F., Serva, L., Vittori, E., 1996. Trench investigations of the 1915 Fucino earthquake fault scarps (Abruzzo, Central Italy): geological evidence of large historical events. Journal Geophysical Research 101, 5921–5936.
Molnar, P., 2001. Climate change, flooding in arid environments and erosion rates. Geology 29, 1071–1074.
Molnar, P., England, P., 1990. Late Cenozoic uplift of mountain ranges and global climate change: chicken or egg? Nature 346, 29–34.
Montgomery, 2001. Slope distributions, threshold hillslopes and steady state topography. American Journal of Science 301, 432–454.
Montgomery, D.R., Stolar, D.B., 2006. Reconsidering Himalayan anticlines. Geomorphology 86, 4–15.
Morewood, N.C., Roberts, G.P., 2002. Surface observations of active normal fault propagation: implications for growth. Journal of the Geological Society, London 159, 263–272.
Mueller, E.R., Pitlick, J., 2005. Morphologically based model of bed load transport capacity in a headwater stream. Journal of Geophysical Research 110, F02016. doi:10.1029/2003JF000117.
Palumbo, L., Benedetti, L., Bourles, D., Cinque, A., Finkel, R., 2004. Slip history of the Magnola fault (Apennines, Central Italy) from Cl-36 surface exposure dating: evidence for strong earthquakes over the Holocene. Earth and Planetary Science Letters 225, 163–176.
Pantosti, D., D'Addezio, G., Cinti, F., 1996. Paleoseismicity of the Ovindoli–Pezza fault, central Apennines, Italy: a history including a large, previously unrecorded earthquake in the Middle Ages (860–1300 A.D.). Journal of Geophysical Research 101, 5937–5960.
Papanikolaou, I.D., Roberts, G.P., Michetti, A.M., 2005. Fault scarps and deformation rates in Lazio-Abruzzo, Central Italy: comparison between geological fault slip-rate and GPS data. Tectonophysics 408, 147–176.
Patacca, E., Sartori, R., Scandone, P., 1990. Tyrhhenian basin and Apenninic arcs: kinematic relations since late Tortonian times. Memorie della Societa Geological Italiana 45, 425–451.
Pizzi, A., 2003. Plio-Quaternary uplift rates in the outer zone of the central Apennines fold and thrust belt, Italy. Quaternary International 101–102, 229–237.
Roberts, G.P., Michetti, A.M., 2004. Spatial and temporal variations in growth rates along active normal fault systems: an example from Lazio-Abruzzo, central Italy. Journal of Structural Geology 26, 339–376.
Roberts, G.P., Cowie, P., Papanikolaou, I., Michetti, A.M., 2004. Fault scaling relationships, deformation rates and seismic hazards. An example from Lazio-Abruzzo, central Italy. Journal of Structural Geology 26, 377–398.
Roe, G.H., Montgomery, D.R., Hallet, B., 2002. Effects of precipitation variations on the concavity of steady state river profiles. Geology 30, 143–146.
Roering, J.J., Kirchner, J.W., Dietrich, W.E., 1999. Evidence for nonlinear, diffusive sediment transport on hillslopes and implications for landscape morphology. Water Resources Research 35, 853–870.
Seidl, M.A., Dietrich, W.E., Kirchener, J.W., 1994. Longitudinal profile development into bedrock; an analysis of Hawaiian channels. Journal of Geology 102, 1994.
Selby, M.J., 1980. A rock mass strength classification for geomorphic purposes, with tests from Antarctica and New Zealand. Zeitshrift fur Geomorphologie 24, 31–51.
Sklar, L., Dietrich, W.E., 1998. River longitudinal profiles and bedrock incision models: stream power and the influence of sediment supply. In: Tinkler, K.J., Wohl, E.E. (Eds.), Rivers Over Rock. AGU Monograph, vol. 107, pp. 272–279.
Snyder, N.P., Whipple, K.X., Tucker, G.E., Merrits, D.J., 2000. Landscape response to tectonic forcing: digital elevation model analysis of stream profiles in the Mendocino triple junction region, Northern California. Geological Society of America Bulletin 112, 1250–1263.
Snyder, N.P., Whipple, K.X., Tucker, G.E., Merritts, D.J., 2003. Importance of a stochastic distribution of floods and erosion thresholds in the bedrock incision problem. Journal of Geophysical Research 108 (B2), 2117. doi:10.1029/2001JB001655.
Stock, J.D., Dietrich, W.E., 2003. Valley incision by debris flows, evidence of topographic signature. Journal of Geophysical Research 39, 1089. doi:10.1029/2001WR001057.
Stock, J.D., Montgomery, D.R., 1999. Geologic constraints on bedrock incision using the stream power law. Journal of Geophysical Research 104, 4983–4993.
Tarboton, D.G., Bras, R.L., Rodriquez-Iturbe, I., 1991. On the extraction of channel networks from digital elevation data. Hydrological processes 5, 81–100.
Tomkin, J.H., Brandon, M.T., Pazzaglia, F.J., Barbour, J.R., Willet, S.D., 2003. Quantitative testing of bedrock incision models for the Clearwater River, NW Washington State. Journal of Geophysical Research 108 (B6), 2308. doi:10.1029/2001JB000862.
Tucker, G.E., Bras, R.L., 1998. Hillslope processes, drainage density and landscape morphology. Water Resources Research 34, 2751–2764.
Tucker, G.E., Whipple, K.X., 2002. Topographic outcomes predicted by stream erosion models: sensitivity analysis and inter-model comparison. Journal of Geophysical Research 107 (B9), 2179. doi:10.1029/2001JB000162.
Tucker, G.E., Lancaster, S.T., Gasparini, N.M., Bras, R.L., 2001. The Channel-Hillslope Integrated Landscape Development (CHILD) model. In: Harmon, R.S., DoeIII III, W.W. (Eds.), Landscape erosion and evolution modeling. Kluwer Academic/Plenum Publishers, pp. 349–388.
Van der Beek, P., Bishop, P., 2003. Cenozoic river profile development in the upper lachan catchment (SE Australia) as a test of quantitative fluvial incision models. Journal of Geophysical Research 108 (B6), 2309. doi:10.1029/2002JB002125.
Weissel, J.K., Seidl, M.A., 1998. Inland propagation of erosional escarpments and the river profile evolution across the southeast Australian passive continental margin. In: Wohl, E., Tinkler, K. (Eds.), Rivers over Rock: Fluvial processes in Bedrock Channels. AGU monograph, vol. 107, pp. 189–206.
Whipple, K.X., 2004. Bedrock rivers and the geomorphology of active orogens. Annual review of earth and planetary sciences 32, 151–185.
Whipple, K.X., Tucker, G.E., 1999. Dynamics of the stream power incision model: implications for the height limits of mountain ranges, landscape response timescales and research needs. Journal of Geophysical Research 104, 17,661–17,674.
Whipple, K.X., Tucker, G.E., 2002. Implications of sediment-flux dependent river incision models for landscape evolution. Journal of Geophysical Research 107 (B2). doi:10.1029/2000JB000044.
Whipple, K.X., Hancock, G.S., Anderson, R.S., 2000. River incision into bedrock: mechanics and relative efficacy of plucking, abrasion and cavitation. Geological Society of America Bulletin 112, 490–503.
Whittaker, A.C., Cowie, P.A., Attal, M., Tucker, G.E., Roberts, G., 2007a. Bedrock channel adjustment to tectonic forcing: implications for predicting river incision rates. Geology 35, 103–106.
Whittaker, A.C., Cowie, P.A., Attal, M., Tucker, G.E., Roberts, G., 2007b. Contrasting transient and steady state rivers crossing active normal faults: new field observations from the central Apennines, Italy. Basin Research 19, 529–556.
Willett, S.D., Brandon, M.T., 2002. On steady states in mountain belts. Geology 30, 175–178.
Wobus, C.W., Hodges, K.V., Whipple, K.X., 2003. Has focused denudation sustained active thrusting at the Himalayan topographic front? Geology 31, 861–864.
Wobus, C.W., Whipple, K.X., Kirby, E., Snyder, N., Johnson, J., Spyropolou, K., Crosby, B., Sheehan, D., 2006. Tectonics from topography: procedures, promise, pitfalls. In: Willet, S., Hovius, N., Brandon, M., Fisher, D. (Eds.), Tectonics, climate and landscape evolution. GSA special paper, vol. 398, pp. 55–74.